DOT/FAA/AR-03/37

Office of Aviation Research
and Development
Washington, D.C. 20591

Advanced Aircraft Materials, Engine Debris Penetration Testing

December 2005

Final Report

This document is available to the U.S. public through the National Technical Information Service (NTIS), Springfield, Virginia 22161.



U.S. Department of Transportation
Federal Aviation Administration

NOTICE

This document is disseminated under the sponsorship of the U.S. Department of Transportation in the interest of information exchange. The United States Government assumes no liability for the contents or use thereof. The United States Government does not endorse products or manufacturers. Trade or manufacturer's names appear herein solely because they are considered essential to the objective of this report. This document does not constitute FAA certification policy. Consult your local FAA aircraft certification office as to its use.

This report is available at the Federal Aviation Administration William J. Hughes Technical Center's Full-Text Technical Reports page: actlibrary.tc.faa.gov in Adobe Acrobat portable document format (PDF).

Technical Report Documentation Page

1. Report No.	2. Government Accession No.	3. Recipient's Catalog No.
DOT/FAA/AR-03/37		

4. Title and Subtitle	5. Report Date
ADVANCED AIRCRAFT MATERIALS, ENGINE DEBRIS PENETRATION TESTING	December 2005
	6. Performing Organization Code NAWCWD 418300D
7. Author(s) Steven J. Lundin and Richard B. Mueller	8. Performing Organization Report No.
9. Performing Organization Name and Address Commander Naval Air Warfare Center Weapons Division 1 Administration Way China Lake, CA 93555-6001	10. Work Unit No. (TRAIS) 11. Contract or Grant No.
12. Sponsoring Agency Name and Address U.S. Department of Transportation Federal Aviation Administration Office of Aviation Research Washington, DC 20591	13. Type of Report and Period Covered Final Report 14. Sponsoring Agency Code ANE-110, ANM-100

15. Supplementary Notes

The Federal Aviation Administration Airport and Aircraft Safety R&D Division Technical Monitor was Donald Altobelli.

16. Abstract

This report documents the results of testing conducted in July and August 2001 at the Naval Air Warfare Center-Weapons Division, China Lake, CA, as part of the continued effort to characterize uncontained engine events. This effort was performed in support of the Federal Aviation Administration Aircraft Catastrophic Failure Prevention Program. Data generated from this test will support the penetration equation development for the Uncontained Engine Debris Damage Analysis Model (UEDDAM), a developmental design tool for conducting aircraft safety analysis for engine rotor burst events.

This testing investigated composite materials and metals for use in component shielding applications. Previous testing had focused on aircraft skins and structural components.

Four materials were investigated during this series of testing: 2024-T351 aluminum, Ti-6Al-4V titanium, Inconel® 625 low-cycle fatigue, and a generalized composite. Impact data from these materials was used to characterize the ballistic response via a material constant within the penetration equations. This material property was previously denoted as the dynamic shear modulus (G_d). Examination of the ballistic limit equation used within the UEDDAM has determined that the material constant is more appropriately a shear constant (C_s).

17. Key Words	18. Distribution Statement
Penetration testing, Uncontained engine debris, Fuselage penetration	This document is available to the public through the National Technical Information Service (NTIS), Springfield, Virginia 22161.

19. Security Classif. (of this report)	20. Security Classif. (of this page)	21. No. of Pages	22. Price
Unclassified	Unclassified	92	

TABLE OF CONTENTS

		Page
EXECUTIVE SUMMARY		ix
1.	INTRODUCTION	1
1.1	Purpose	1
1.2	Background	1
2.	TEST OBJECTIVES	2
3.	APPROACH	3
3.1	Test Overview	3
3.2	Test Sequence	7
3.2.1	Phase I: Composite Materials	7
3.2.2	Phase II: Component Shielding Materials	9
4.	DATA ANALYSIS	10
4.1	Velocity Calculation	10
4.2	Presented Area	12
4.3	Penetration Equations	13
4.3.1	Penetration Mechanics	14
4.3.2	Ballistic Limit Equation	17
4.3.3	Residual Velocity Equation	22
4.4	Shear Coefficient Methodology	22
5.	RESULTS	24
5.1	Generalized Composite	24
5.2	2024-T351 Aluminum	29
5.3	Ti-6Al-4AV Titanium	32
5.4	Inconel 625 LCF	36
5.5	Shear Parameter Discussion	38
6.	CONCLUSION	39

7. RECOMMENDATIONS 40

8. REFERENCES 41

APPENDICES

A—Detailed Test Plan
B—Complete Test Data

LIST OF FIGURES

Figure		Page
1	Nitrogen-Powered Gas Gun	4
2	A 12″ Bore Barrel Extension	4
3	Stripping of Sabot From Fragment	5
4	Test Stand	5
5	Test Lighting Setup	7
6	Composite Panel Lay-Up	8
7	Presented Area Analysis Tool	13
8	Plugging Penetration Mode	14
9	Petaling Penetration Mode	14
10	Fragment Presented Area	15
11	Fragment Impact Angle	16
12	Fragment Impact and Obliquity Angles	17
13	Integration Range for Cylindrical Plugging Model	19
14	Generalized Composite Panel Density with Respect to Thickness	27
15	Composite Panel Ballistic Analysis Thickness	27
16	Experimental Correlation for Composite Panels	28
17	Minor Composite Panel Damage	28
18	Major Composite Panel Damage	29
19	Exeperimental Correlation for Aluminum Panels	31
20	Fragment Deformation Due to Impact	31
21	Panel Damage Due to Fragment Deformation	32
22	Panel Damage at Ballistic Limit	32
23	Experimental Correlation for Ti-6Al-4V Titanium Panels	34
24	Fragment Breakup for Shot 20	35
25	Panel Damage for Shot 20	35
26	Fragement Deformation for Shot 21	36
27	Panel Damage for Shot 21	36
28	Experimental Correlation for Inconel 625 LCF Panels	38

LIST OF TABLES

Table		Page
1	Composite Panel Honeycomb Thickness and Quantities	8
2	2024-T351 Aluminum Panel Thickness and Quantities	9
3	Ti-6Al-4V Titanium Panel Thickness and Quantities	10
4	Inconel 625 LCF Panel Thickness and Quantities	10
5	Comparison of Material Constants	21
6	Composite Panel Impact—Physical Data	25
7	Composite Panel Impact—Dynamic Data	26
8	2024-T351 Aluminum Panel Impact—Physical Data	29
9	2024-T351 Aluminum Panel Impact—Dynamic Data	30
10	Ti-6Al-4V Titanium Panel Impact—Physical Data	33
11	Ti-6Al-4V Titanium Panel Impact—Dynamic Data	34
12	Inconel 625 LCF Impact—Physical Data	37
13	Inconel 625 LCF Impact—Dynamic Data	37
14	Comparison of Material Properties	39
15	Material Shear Strength (C_s) Summary	40

LISTOF ACRONYMS AND SYMBOLS

2-D	Two-dimensional
3-D	Three-dimensional
ACFPP	Aircraft Catastrophic Failure Prevention Program
COVART	Computation of Vulnerable Area and Repair Time
C_s	Shear constant
DoD	Department of Defense
FAA	Federal Aviation Administration
FASTEGEN	Fast Shotline Generator
Fps	Feet per second
G_d	Dynamic shear modulus
HS	High speed
JTCE/ME	Joint Technical Coordinating Group on Munitions Effectiveness
KE	Kinetic energy
LCF	Low-cycle fatigue
NAWC-WD	Naval Air Warfare Center-Weapons Division
MS	Microsoft
pps	Pictures per second
rms	Root mean square
SI	System International
UEDDAM	Uncontained Engine Debris Damage Assessment Model
UEDMP	Uncontained Engine Debris Mitigation Program
V_{50}	Ballistic limit equation
V_r	Residual velocity
VUs	Vanguard Units

EXECUTIVE SUMMARY

This work was conducted under the sponsorship and oversight of the Federal Aviation Administration (FAA) Engine and Propeller Directorate and the Transport Airplane Directorate. The Uncontained Engine Debris Mitigation Program falls under the Aircraft Catastrophic Failure Prevention Program, which is led by the Airport and Aircraft Safety Research and Development Division located at the FAA William J. Hughes Technical Center, Atlantic City International Airport, New Jersey.

A series of tests were conducted during July and August 2001 at the Naval Air Warfare Center-Weapons Division, China Lake, CA, as part of the continued effort to characterize uncontained engine events. This testing was performed to aid development of the Uncontained Engine Debris Damage Analysis Model (UEDDAM), a developmental design tool for uncontained engine event safety analysis. The UEDDAM uses a set of penetration equations to estimate ballistic impacts on aircraft structure and skins from engine fragments. Contained within the penetration equations is an empirical constant that defines the ballistic response of the target metal.

The previous empirical constant, dynamic shear modulus, was known only for three metals of unspecified alloys for aluminum, titanium, and steel. A goal of this testing was to determine the empirical constant for specific aircraft materials. The results of the testing and analysis are contained within this report. Materials constants have been specified for the following: 2024-T351 aluminum, Ti-6Al-4V titanium, Inconel® 625 low-cycle fatigue, and a generalized composite.

These tests have resulted in increasing the number of materials that may be handled by the penetration model, increased confidence in their applicability to thick barriers, and evidence that those materials tested here may be easily modeled. This work has developed a methodology that, given the goal of finding a very simple and computationally fast form, provides very good agreement for the test data analyzed to date.

1. INTRODUCTION.

1.1 PURPOSE.

This test series was conducted to validate the previously accepted dynamic shear modulus (G_d) values for aluminum and titanium materials [1] and to determine the G_d values for a nickel-based superalloy and generalized graphite composite. This penetration data is used within the Uncontained Engine Debris Damage Assessment Model (UEDDAM) for the prediction of ballistic impacts. G_d is the parameter used within the ballistic limit (V_{50}) equation to quantify the ballistic response of the target material. Specifically, the penetration equations are used to determine whether a penetration will occur (V_{50}), and if so, what velocity the fragment will maintain afterwards (residual velocity V_r). This testing will provide fragment impact data on the following materials: 2024-T351 aluminum, Ti-6Al-4V titanium, Inconel® 625 low-cycle fatigue (LCF), and a generalized composite. This report documents the testing conducted and the subsequent analysis of the G_d, for the aforementioned materials. (The dynamic shear modulus will be shown later to be a misnomer and is more accurately termed shear constant, C_s).

1.2 BACKGROUND.

The Federal Aviation Administration (FAA) initiated a research program, the Uncontained Engine Debris Mitigation Program (UEDMP), to investigate and determine methods to mitigate the damage caused by uncontained engine debris. Damage from such an event is often considerable, but not necessarily be catastrophic as long as structural integrity is maintained, fires are not sustained, and critical systems do not become inoperable. The UEDMP, managed by the Airport and Aircraft Safety Research and Development Division located at the FAA William J. Hughes Technical Center, Aircraft Catastrophic Failure Prevention Program (ACFPP), works with industry and government to determine possible engineering solutions to reduce injuries and critical damage resulting from uncontained engine events. As part of this program, the Naval Air Warfare Center-Weapons Division (NAWC-WD) was tasked to evaluate ballistic damage analysis tools and vulnerability (damage) reduction techniques currently in use within the Department of Defense (DoD).

The UEDDAM tool was developed as an aircraft design and certification tool to address the uncontained engine debris hazard. Using the existing DoD tools for aircraft vulnerability analysis (Computation of Vulnerable Area and Repair Time (COVART) and Fast Shotline Generator (FASTGEN)), these codes were modified to describe engine fan blade fragments and to permit unlimited distribution of the tools. Within the UEDDAM, the penetration equations are used to determine the result of impacts to aircraft skin and components along the path of the fragment. Testing has provided the fragment penetration characteristics in terms of fragment orientation at impact, impact velocity, and fragment residual velocity.

Testing at NAWC-WD has been conducted in support of the UEDDAM code, specifically in developing the penetration equations to model the impacts of engine fan blades. Three series of tests have been completed to date.

The first test series investigated small (less than 2″ square) to medium-sized (3″ by 8″) fragments impacted into aluminum plates and engine cowlings [2]. Performed in 1998, this early testing

also investigated the prediction accuracy of several ballistic impact prediction methods, accepting both the Joint Technical Coordinating Group on Munitions Effectiveness (JTCG/ME), residual velocity (V_r), and ballistic limit (V_{50}) equations as reasonable prediction tools for fan blade impacts.

The second series, the following year, investigated small to medium-sized fragments impacted into an actual narrow-body commercial aircraft fuselage, denoted as Fuselage Test Phase I [3].

The third series, in 2000, impacted medium to large-sized (8″ by 8″) fragments into the same fuselage [4]. During the fuselage testing, the interaction of various aircraft structural elements created some disparity in the accuracy of the predictions of the penetration equations. Analysis of this phenomena determined that the V_{50} equation developed from the FAA Energy Equation 1 was a more effective prediction tool for both single skin and complex structural impacts.

All three test series had principally impacted 2024-T3 aluminum. A degree of confidence in predicting the effect of fragment impacts into aircraft skins and complex structures has been attained in addition to an effective test procedure and analysis methodology. Consequently, the next effort would further the prediction capabilities of the UEDDAM through the examination of different materials and applications other than the aircraft skin.

Composite materials are being incorporated into most modern aircraft. Variations in aircraft construction using composites make it difficult to characterize the ballistic response of this material. Therefore, ballistic characterization of composites should be limited to those in areas that are susceptible to uncontained engine debris. The effectiveness of using the penetration equations to predict impacts into an anisotropic material should also be evaluated.

The current test series investigated four materials: 2024-T3 aluminum, Ti-6Al-4V titanium, Inconel 625 LCF, and a generalized composite. Previous testing determined that the material constant, G_d, (210 MPa for aluminum) provided effective predictions for the 2024-T3 alloy type [4]. Current testing would determine the validity of this existing material constant for the prediction of fragment impacts into thicker panels (0.250″-0.375″). Fragment impact data on Ti-6Al-4V will determine the effectiveness of applying the existing G_d value of 996 MPa into thicker materials for use in component shielding applications [1]. This value of G_d is not specifically stated in reference 1, but is referred to as a ratio of the shear strength for aluminum. Analysis of the test data shall attempt to determine the G_d for the generalized composite and Inconel 625 LCF.

2. TEST OBJECTIVES.

The objective of this test was to obtain fragment impact data for composite skin materials and metals being considered for component shielding applications. Test data is intended to support the development and validation of the penetration equations to predict engine fan blade impacts into these advanced materials. Specific impact data to be measured was fragment impact velocity, fragment impact orientation, and fragment residual velocity.

3. APPROACH.

The overall approach used in this project was to determine the test article specifications (composite lay-up, and material thickness), to develop test parameters (velocities and impact orientations), to perform ballistic testing, and to analyze the test data to either validate or develop the penetration equations.

The test article specifications were selected to provide the most generally applicable, but useful results. For example, the composite panel lay-up was designed to be representative of those submitted by industry partners and resulted in three different Nomex® honeycomb thicknesses. The component shielding material thicknesses were selected to be greater than those previously tested. With the exception of the Inconel, two different thicknesses were tested for the purposes of obtaining a broader database.

The test parameters were selected to provide the most effective and efficient use of materials and results for each material. For the composite panels, testing was done in an attempt to characterize the ballistic response of the material so that the penetration equations could be applied with a sufficient degree of confidence. The matrix for the composite materials desired that for each honeycomb thickness, two fragment sizes, each projected at two different fragment angles, and each at three different velocities, were to be tested. The emphasis on testing the component shielding materials was to provide the greatest challenge to the test panel. For all metal panels, only the 8″ by 8″ fragments were tested, impacting at an edge-on condition (90° fragment angle), with the shotline (fragment trajectory path) perpendicular to the panel (0° obliquity). Velocities selected for the component shielding materials were in the region of the estimated V_{50} for each material.

Ballistic testing was categorized into two phases: composite materials and component shielding materials. In the execution of the test, these two phases were merged for economy reasons.

Analysis of the test data served to verify the performance of the penetration equations in predicting the V_{50} and residual velocities for 2024-T351 aluminum and Ti-6Al-4V titanium. Empirical coefficients (G_d) existed for both materials [1], but the effectiveness of the equations for materials thicker than the standard aircraft skins had not been verified.

The purpose of the test data analysis for the Inconel 625 LCF and composite materials was to obtain enough empirical data to characterize their ballistic response sufficiently so that a material constant could be determined. The emphasis for the composite material was to characterize the residual velocity because it was predicted that such thin material would offer only marginal resistance to penetration. With the Inconel 625 LCF, the V_{50} was considered more important due to its intended use in component shielding.

3.1 TEST OVERVIEW.

Testing was performed at the Weapons Survivability Laboratory facility in China Lake, CA. All testing was performed on the C-2 section of the main test pad from 23 July to 15 August 2001. The major components of the test setup were a nitrogen-powered gas gun, the test panel stand, background boards, and two 16-mm, high-speed (HS) cameras.

A nitrogen-powered gas gun was used to shoot the fan blade fragments into the test panels (figure 1). For this test, the fragments were in the 0.5- to 1.5-lb range and were projected at velocities between 150-800 frames per second (fps).



FIGURE 1. NITROGEN-POWERED GAS GUN

The 12″ bore barrel extension was attached to the gas gun to enable testing of the 8″ by 8″ sized fragments, as shown in figure 2. Nominal bore size of the gun is 6.07″. The barrel extension was an existing piece of equipment that had been designed for a previous test under the FAA ACFPP. This barrel extension was used throughout the test, even for the 3″ by 8″ sized fragments, to standardize the fabrication of only one sabot size.

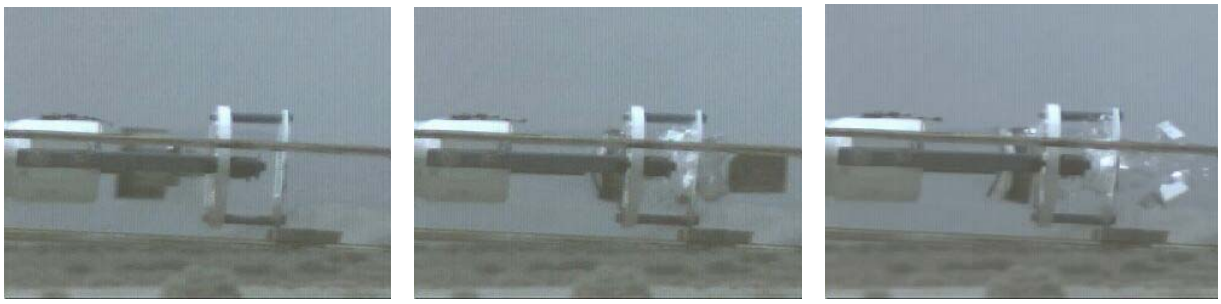


FIGURE 2. A 12″ BORE BARREL EXTENSION

The sabot is required to launch the fan blade fragments from the gun. The sabot allows subcaliber and unconventional-shaped objects to be launched from the gun. For this test, the sabot construction consisted of three components: Teflon® base plate, steel sabot ring, and foam filler. A Teflon base plate is used to seal the bore, transferring the load from the pressurized gas

to the sabot. A steel ring, fabricated from thin sheet, acts as an interface between the foam and the barrel while the foam is the filler around the projectile, which is easy to cut and light enough so that it falls to the ground after separation.

A double-baffled sabot stripper was attached to the muzzle of the 12″ bore extension. Operation of the sabot stripper is shown in the sequence of HS video frames in figure 3. The sabot exits the barrel, figure 3(a), then impacts the first baffle of the stripper and stops. The projectile continues forward through the opening in the stripper, figure 3(b). With the foam separated from the projectile, it looses momentum, figure 3(c). Adding a second baffle to the sabot stripper was a precautionary measure designed to restrain the base plate if it manages to twist through the first baffle. If the base plate were to come loose, it could damage the lighting equipment arranged close to the shotline.



(a) (b) (c)

FIGURE 3. STRIPPING OF SABOT FROM FRAGMENT

The test stand was specially designed for this test to retain 36″ square panels rigidly. Two load-spreading rails retained the panels along the top and bottom of the frame. Eyelets on the frame were used to secure the stand to the test pad with steel cables. Figure 4 shows an engineering drawing of the test stand. An additional feature of the design was that it allowed for an unobstructed field of view for the HS cameras on both the entrance (impact) and exit (residual) sides of the test panel.

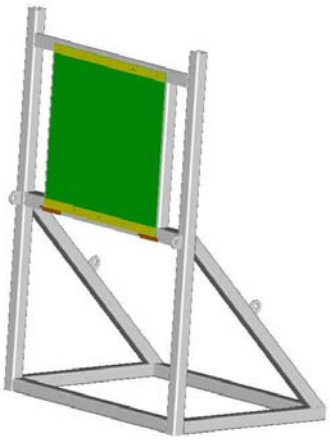


FIGURE 4. TEST STAND

A bundle of Celotex® was placed in the shotline behind the test panel to capture the fan blade fragment for reuse. This material comes in a palletized form and was replaced during the test as it deteriorated through use.

Data required from each test shot included the impact and residual velocities of the fragments and the impact orientation of each fragment with respect to the target. This data was obtained from HS film. Two cameras were used, one to view the front side of the panel (initial velocity, V_i, and fragment orientation, θ) and a second camera to view the aft panel side (V_r). The cameras were Photec 16-mm film, capable of 10,000 fps. For this test, the frame rate was set at 6000 pictures per second (pps). To achieve a frame rate of 6000 fps, the cameras had to be initiated 1.8 (±0.2) seconds prior to the impact. This was achieved through the use of a sequencer, with the time (t=0) supplied by either the gun firing signal or a break-wire on the muzzle. The desired method was to initiate the sequencer from the break-wire signal due to the inconsistencies in the electrical and mechanical delays in the gun firing system. This delay was often in the 30-50 millisecond region, whereas the break-wire signal was almost instantaneous. Inconsistencies in t=0 were less of a problem for the HS cameras than it was for the flash bulb timing.

Supporting the 16-mm film cameras was one 512- by 512-pixel digital HS camera. This camera had not been used previously and, therefore, was used for trials purposes only. However, velocity measurements were obtained for two shots where the film cameras had failed. The digital camera had several advantages over the film cameras in regard to triggering pulse and exposure settings, in addition to the obvious lack of time and cost involved in processing film. A triggering pulse could be sent to the camera, where the camera software was capable of setting a delay offset, thus eliminating the need for a sequencer. The software was also capable of adjusting exposure time, a mechanical function on the Photec cameras that was dependent on camera speed and F-stop setting. However, the major drawback to this system was the low resolution compared to the 16-mm film and Vanguard Motion Analyzer. This loss of resolution would have little effect on velocity calculation, but would considerably reduce fidelity in fragment orientation measurement.

The shotline was lit with a combination of flash bulbs and sealed beam lamps. A total of six MegaFlash 6M Lumen flash bulbs were used in two banks of three on either side of the test panel (see figure 5). From previous testing, the performance of this brand of flash bulbs had been characterized as 0.15 ms of warmup, with an effective lighting duration of 44 ms. This warmup time required the use of the sequencer to initiate. As mentioned previously, inconsistencies existed when using the gun firing pulse for t=0. All flash bulbs were focused on the shotline and impact area. To provide area fill for the background and minimal lighting in the event of a timing error for the flash bulbs, twelve 1000 W incandescent PAR64 lamps were used. These PAR64 lamps came in two banks of six, with one bank in both the front and rear of the test panel.



FIGURE 5. TEST LIGHTING SETUP

3.2 TEST SEQUENCE.

The test plan outlined a total of 55 test panels, divided into two different test series: composite materials and component shielding metals. The original test matrix can be seen in the test plan enclosed in appendix B. In actual testing, a total of 64 panels were tested as follows:

- 29 Generalized Composite Panels
  - 12 panels 0.250″ Nomex honeycomb
  - 12 panels 0.375″ Nomex honeycomb
  - 5 panels 0.500″ Nomex honeycomb
- 35 Component Shielding Materials
  - 6 panels 0.063″ Inconel 625 LCF
  - 4 panels 0.063″ Ti-6Al-4V titanium
  - 5 panels 0.125″ Ti-6Al-4V titanium
  - 5 panels 0.250″ Ti-6Al-4V titanium
  - 10 panels 0.250″ 2024-T351 aluminum
  - 5 panels 0.375″ 2024-T351 aluminum

3.2.1 Phase I: Composite Materials.

Ballistic testing of metal and composite panels was performed, impacting fan blade fragments at velocities representative of an uncontained engine debris event. All fan blade fragments used in testing were in the 0.5- to 1.5-lb range and were fabricated from actual engine fan blades supplied by an engine manufacturer. Fragment impact velocities ranged from 200-800 fps.

The Phase I testing was performed on 29 composite panels. These panels were specifically fabricated for this test from a generalized lay-up. Several composite lay-up specifications were received from industry for composite structures used in engine nacelles and other aircraft regions where uncontained engine events may impact. The final lay-up was selected as being the most representative of those submitted by industry. For aviation use, most composite lay-ups contained a metal-impregnated graphite layer in the lay-up for conductivity. The metalized layer was omitted in the test panels because it neither contributed to the strength of the material nor to the economy of construction. The generalized lay-up consisted of three symmetric angle-ply layers of graphite on either side of a Nomex honeycomb center, as shown in figure 6. Three different honeycomb thicknesses were tested: 0.250″, 0.375″, and 0.500″. The quantities of panels for each honeycomb thickness are shown in table 1. To provide a database that was comprehensive enough to determine the shear strength for composite materials, the test matrix was setup to investigate two fragment angles and three different velocities for each thickness of honeycomb.

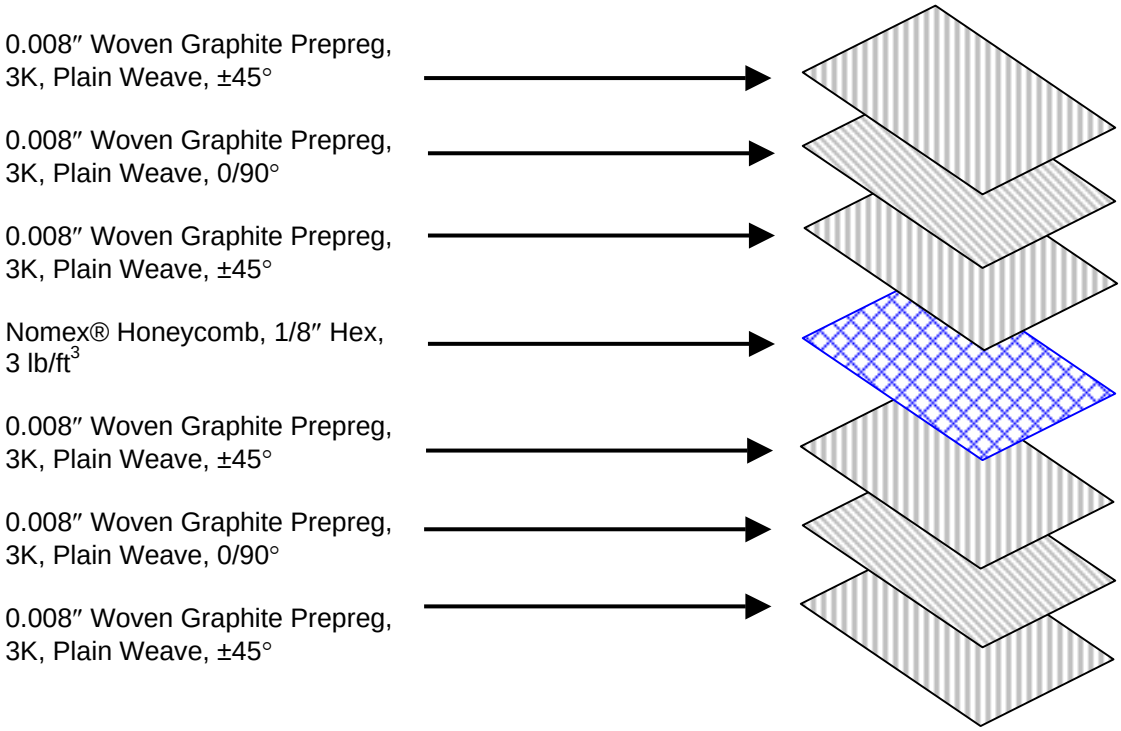


FIGURE 6. COMPOSITE PANEL LAY-UP

TABLE 1. COMPOSITE PANEL HONEYCOMB THICKNESS AND QUANTITIES

Nomex Honeycomb Thickness (in.)	Quantity
0.250	12
0.375	12
0.500	5*

*Six panels were fabricated, but one was damaged during manufacturing.

Composite materials are currently not defined in the penetration equations, and as such, they are not included in the UEDDAM. Testing serves to obtain enough data points to determine the material constant. Phase I testing will also attempt to characterize the ballistic response and penetration mechanics involved during ballistic impacts involving composites.

3.2.2 Phase II: Component Shielding Materials.

The second phase of testing investigated materials that were used in aircraft component shielding. Three metals were tested: Inconel 625 LCF, Ti-6Al-4V titanium, and 2024-T351 aluminum. Previous testing at NAWC-WD, under the UEDMP, had tested both 2024-T3 and 7075-T6 aluminum. During these tests, the thickness of materials investigated did not exceed 0.100″. Current interest within industry is to use shielding to protect critical components from uncontained engine debris, which dictates the need to determine how effective the penetration equations are for panels thicker than a standard aircraft skin.

Testing of the aluminum panels was to determine the effectiveness of the penetration equations when applied to materials thicker than 0.100″. A total of fifteen 2024-T351 aluminum panels were evaluated during this test in two panel thicknesses, 0.250″ and 0.375″. The 2024-T3 and 2024-T351 aluminum have the same material properties but are designated as such to imply that they are sheet and plate products, respectively. Table 2 lists the panel thickness and quantities tested. Impact velocities were selected in the region of V_{50}, with the intention of demonstrating the bounds of a calculated V_{50}. Residual velocities were a secondary concern but were used to further validate the penetrations equations.

TABLE 2. 2024-T351 ALUMINUM PANEL THICKNESS AND QUANTITIES

2024-T351 Aluminum Thickness (in.)	Quantity
0.250	10
0.375	5

The accuracy of the penetration equations for predicting the ballistic response has never been determined for titanium because it was not been previously tested under the FAA ACFPP. The G_d for titanium had been loosely defined as 76.9% of the G_d for steel [1]. However, the exact material properties (alloy types) of titanium and steel were not defined. The titanium investigated in this test series was Ti-6Al-4V. This particular grade of titanium has already been considered for component shielding by an industry partner. A total of 14 panels were tested in three different thicknesses: 0.063″, 0.125″, and 0.250″ (see table 3). Only the 0.125″ and 0.250″ thick panels were tested under the auspices of component shielding. The four 0.063″ thick panels were fabricated from materials already existing at the range and were employed during the system checkout tests. These additional panels provided some supplementary data points to evaluate the titanium.

TABLE 3. Ti-6Al-4V TITANIUM PANEL THICKNESS AND QUANTITIES

Ti-6Al-4V Titanium Thickness (in.)	Quantity
0.063	4*
0.125	5
0.250	5

*Additional panels tested during system checkout tests.

The last metal tested under Phase II was a nickel-chromium-molybdenum alloy known as Inconel 625 LCF. This material is currently in use in engine exhausts and is a fatigue-resistant version of the standard Inconel 625 alloy. Inconel is a relatively new material and due to the specialized applications it is used in was limited in available sheet sizes and thicknesses. At the time of testing (July-August 2001), the thickest available sheet was 0.063″ (see table 4). Impact velocities were selected such that, with a limited amount a data points, a V_{50} could be adequately determined.

TABLE 4. INCONEL 625 LCF PANEL THICKNESS AND QUANTITIES

Inconel 625 LCF Thickness (in.)	Quantity
0.063	6

4. DATA ANALYSIS.

The primary instrumentation device used in this test for data acquisition is the 16-mm, HS film. From posttest film analysis, the fragment impact velocity (V_i) and orientation prior to impact as well as the velocity after impact (V_r) can be determined. Further data is extrapolated from the HS film data, such as fragment angle (θ), presented area (A_p), and presented perimeter (L_p). These parameters provide the inputs for the penetration equations. The film analysis was performed using a Vanguard Motion Analyzer. This equipment allows the user to examine film on a frame-by-frame basis with a set of manually operated cross hairs to locate specific points within a frame. The cross hairs are linked to a counter that gives the horizontal and vertical coordinates within the frame as Vanguard Units (VUs).

4.1 VELOCITY CALCULATION.

Determining the fragment initial and residual velocities from the HS film was performed using the Vanguard Motion Analyzer in a three-step process.

1. Conversion of VUs to unit of length (scaling factor) and any parallax correction (photographic distortion)

2. Determine camera frame rate, in pps, over fragment flight

3. Calculation of fragment velocity

Obtaining data from the HS film requires converting the analyzer cross hair position counter to units of length or, in other words, a scaling factor. This involves measurement on the screen of the motion analyzer (in VUs) of a known length in a frame. Division of the number of VUs on the screen of the motion analyzer by the actual length of the object on the image produces a conversion factor for the data analysis. However, the reference length must be at the same distance from the camera as the shotline or parallax errors are introduced. For this test, the reference length was marked on the grid board behind the shotline, thus requiring a correction to be applied. The correction for parallax was:

$$l_{shotline} = l_{reference}\left(\frac{d_{shotline}}{d_{reference}}\right) \tag{1}$$

where

$d_{reference}$ = distance of reference length from camera
$d_{shotline}$ = distance of shotline from camera
$l_{reference}$ = length of reference length
$l_{shotline}$ = corrected length at shotline

The speed of the camera is determined from timing marks placed on the edge of the film at 1-ms intervals, with a double timing mark at every 10-ms increment. The number of frames between the double-timing marks divided by 0.01 second determines the frame rate or camera speed in pps. Due to the variance in camera speeds, the frame rate data is taken using the same frames that velocity data is to be calculated from to minimize errors.

The final step in determining the fragment speed from the HS film is to determine the number of VUs traveled by the fragment and note the number of frames. The cross hairs of the motion analyzer are placed on the fragment, typically on the center, and the x position noted. For ease of film analysis, a self-adhesive red dot was placed on the center of the fragment to use as the reference point. The film was then stepped forward through frames until the fragment reaches a point similar in distance from the centerline of the frame as the first data point was taken. This distance traveled in VUs is then converted into units of length via the aforementioned scaling factor. The number of frames between the two data points is noted.

Average velocity is then determined by the following equation:

$$V = \frac{r \cdot d}{n} \tag{2}$$

where

d = Distance traveled (m)
n = Number of frames
r = Camera frame rate (fps)
V = Fragment velocity (m/s)

4.2 PRESENTED AREA.

The presented area is also determined from analysis of the HS film via the Vanguard Motion Analyzer. Determination of the fragment orientation is a complex process, but can be broken down into three major steps:

- Selecting corner location coordinates from HS film
- Optimization of viewed fragment area to known fragment dimensions using the Solver function in Microsoft (MS) Excel® 2000
- Calculation of fragment angle, presented area, and presented area perimeter (Lp)

The film image of the fragment prior to impact provides measurements of the corners in the two-dimensional (2-D) image plane. This corner point data is in VUs. Determination of a scaling factor was discussed previously under the procedure for calculating velocities from film data.

The corner point data is then correlated with a computer model of the fragment to find the three-dimensional (3-D) orientation that matches the 2-D projection on the image plane. This process is performed via a custom-written analysis tool in MS Excel 2000, of which a typical screenshot is shown in figure 7. The spreadsheet is setup to input the actual fragment dimensions, corner point data, and film-scaling data. Using the Solver function in Excel, the spreadsheet iterates through fragment rotations until the error between the film data and 2-D solution projections are minimized. The Solver function is an implementation of the Simplex method of solving linear programming problems. By modeling the fragment as a cambered rectangular plate, a simple model can be developed that approximates a 3-D model of the fragment. The camber allows what would otherwise be an infinitely thin plate to exhibit the property of thickness when viewed edgewise along the shotline. The spreadsheet can rotate the model in 3-D space. For any set of ordered rotations, the view along the camera line should have an orientation for which the corner data produces a minimum error to the measured data. The Solver finds the minimum error between the model corners to the measured corner data by varying the rotation angle on each of the three axes. The model and the measured data are normalized into the same unit space prior to error calculation.

Using a single view will produce a valid presented area, but the exact orientation of the fragment will be ambiguous in the direction parallel to the shotline (roll axis). That ambiguity is resolved by examining pictures of the actual impact. For example, the Solver might determine a roll angle (φ) of 20° or -20°. Observing the impact hole from pictures of the shot allows the analyst to quickly assign the correct sign to the angle.

The perimeter of the presented area is obtained via vector analysis computation for the area of a parallelogram applied to each of the model elements in the shotline projection. The camera setup geometry provides the parallax correction to the high-speed image data. The error, due to perspective, is not accounted for because it is very small compared to the image blur and parallax.

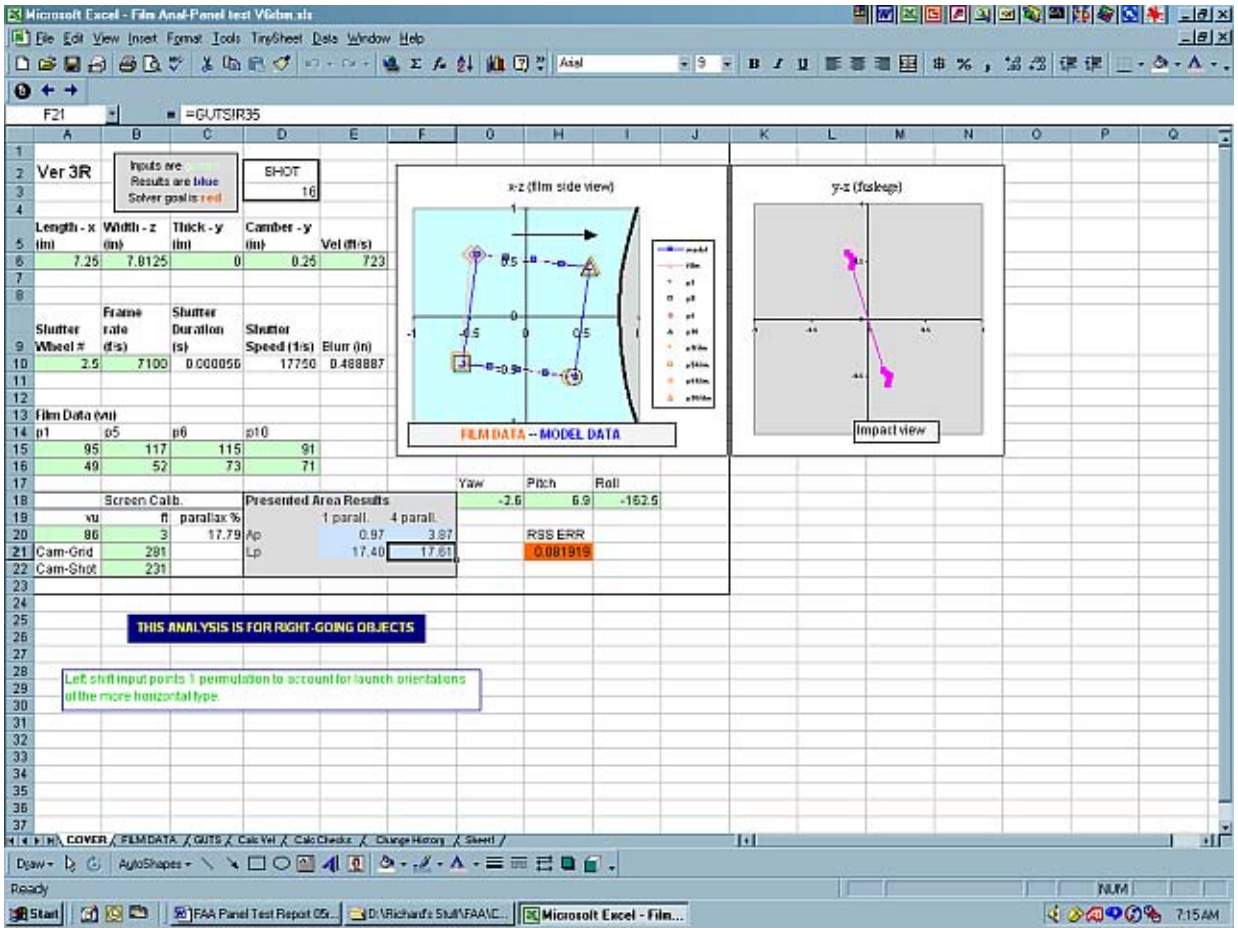


FIGURE 7. PRESENTED AREA ANALYSIS TOOL

The use of a single-camera view for measurement may leave an ambiguity in the exact fragment orientation. However, from previous testing experience, it has been found that two camera views are difficult to manage in large test setups. Therefore, this data collection and analysis methodology has been developed based on the use of a single-camera view.

4.3 PENETRATION EQUATIONS.

The UEDDAM code uses a set of penetration equations to predict the damage to an aircraft structure from an engine fragment along a given shotline. The equations used within the UEDDAM have been optimized through the evaluation of previous testing under the ACFPP. Two equations are required to describe a ballistic penetration: the V_{50} and the V_r. Several sources and versions of penetration prediction tools exist. The UEDDAM uses the residual velocity equation developed by the JTCG/ME and the ballistic limit equation from the FAA. It must be noted that due to the empirical nature of the penetration equations, it is critical that the correct units are entered into the equations. Thus, the correct units will be defined in this section.

4.3.1 Penetration Mechanics.

Ballistic penetrations can be described as two basic modes and a combination thereof: plugging and petaling. The plugging mode typically occurs for blunt objects and for sharp objects at large yaw angles. Upon impact, the shearing force becomes great along the perimeter of the fragment, such that a failure occurs and a plug of material is removed. This plug is accelerated in the direction of the fragment and, thus, is involved in removing some of the energy from the impact. Figure 8 shows the plugging phenomenon.

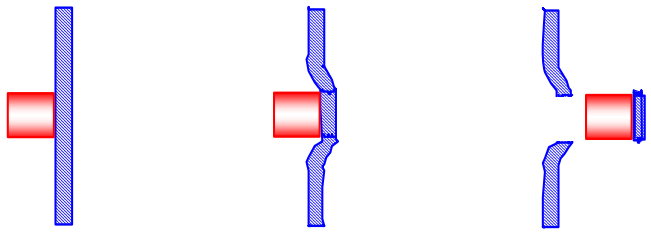


FIGURE 8. PLUGGING PENETRATION MODE

Petaling occurs typically for sharp projectiles with minimal yaw, where the contact edge creates an intense shear stress over a small region in the impact area. This results in an initial rupture of the target material. After the initial piercing, the material remains attached but is deformed as the rest of the fragment continues through the target material. Figure 9 shows this process. The petaling mode of penetration removes less energy from the fragment than plugging.

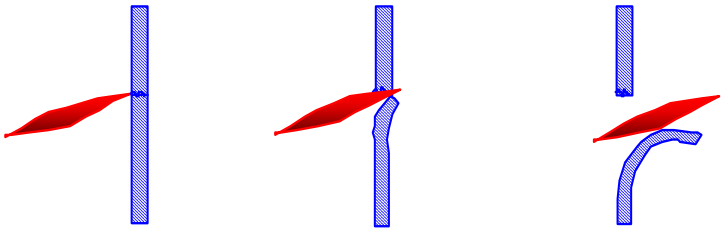


FIGURE 9. PETALING PENETRATION MODE

In reality, most penetration modes are combinations of plugging and petaling. There are many impact conditions that affect the mechanics of penetration. These factors can be categorized as follows:

- Projectile/fragment physical properties
  - Dimensions
  - Shape (blunt or sharp object)
  - Mass
  - Material composition (frangibility)

- Ballistic properties
  - Impact velocity
  - Fragment orientation
  - Shotline obliquity
  - Presented area
- Impacted element's properties
  - Material
  - Thickness

These parameters are addressed within the penetration equations. Definitions of each factor are described below, as they are used for the penetration equations.

The fragment shape and orientation are important factors in a ballistic impact. These two factors determine the presented area of the fragment at impact. Presented area is the area along the projectile's trajectory that is seen by the target material (see figure 10). For a projectile such as a bullet, this is essentially the cross-sectional area of the cylinder, but for an irregular-shaped projectile, the presented area can change drastically due to yaw. This area is always defined with respect to the plane normal to the fragment trajectory. In the case of impact with obliquity, the projected area and the subtended projected area (hole in the target) will not be identical. In using the equations presented here, it must be understood that the two are different and that the presented area, not the subtended presented area, is used in the estimation of residual velocity. That is because the equation is empirical and its basis is that presented area. There can also be a source of confusion in the perimeter of the presented area in the V_{50} equation. This equation is based on the shear energy and requires the true length of the shear line in the material. Therefore, one must use the perimeter of the subtended presented area in the case of impacts with obliquity to compute V_{50} for the impact. Throughout this analysis, the perimeter of the presented area is taken to mean the perimeter of the subtended presented area.

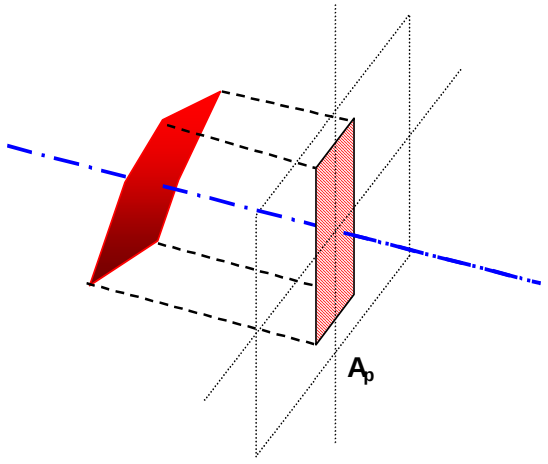


FIGURE 10. FRAGMENT PRESENTED AREA

The fragment mass, *m*, affects the cross-sectional density of the projectile and, thus, the amount of kinetic energy per unit area applied to the target material. The units in the penetration equations for A_p and *m* are m^2 and kg, respectively. The material composition of the impactor is important for the accurate prediction of the ballistic characteristics of incendiary and armor piercing projectiles. This factor does not apply to the solid titanium engine fan blade fragments described under the FAA ACFPP.

The fragment orientation angle is identical to the angle between the target plane and the rotated fragment plane. The coordinate system convention used in calculating the fragment angle (α) is shown in figure 11. This coordinate reference frame is not the same as the system used in the penetration modeling codes. When reading both, it is important to keep in mind the differences in variables and reference systems. The fragment impact angle in 3-D space is found from the dot product of the normal vectors to each plane. In these tests, the obliquity is zero. Given the launch basis or initial conditions, the fragment y-axis unit vector (Y_b) can be rotated through the yaw-pitch-roll Euler angles (Y_b') and then dotted with the initial fragment x-axis unit vector, which is identical to the target x-axis unit vector, to compute the fragment angle. The impact angle is used in determining the A_p and L_p at the time of impact.

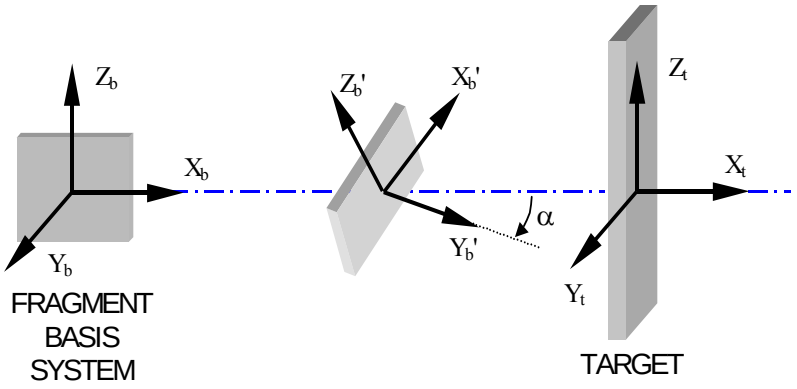


FIGURE 11. FRAGMENT IMPACT ANGLE

The obliquity angle is the angle of incidence between the fragment shotline and the normal to the surface of the target material. The frame of reference for the penetration equations considers a perpendicular to the target surface as a 0° obliquity angle. The sign convention for the obliquity angle is shown in figure 12. For all shots in this test series, the panel was placed perpendicular to the shotline, thus, the obliquity angle was 0°.

The final aspects to be considered in a ballistic penetration are the parameters of the target object: thickness and material type. The thickness of the material in the region of impact is considered to be constant in the penetration equations. The units used for thickness are meters (m). The type of material modeled is described by an empirical constant (formerly known as the dynamic shear modulus, G_d). However, research into this parameter during the analysis of the test data has determined that it is more accurate to name this material parameter as a shear constant (C_s) rather than as a dynamic shear modulus (G_d).

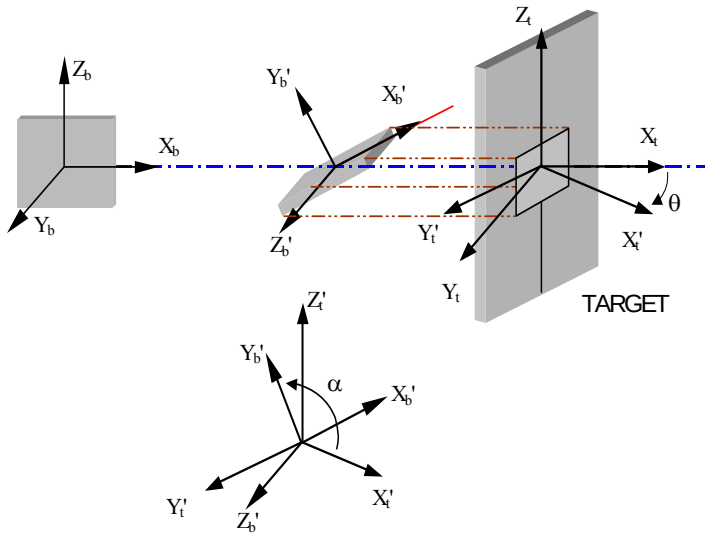


FIGURE 12. FRAGMENT IMPACT AND OBLIQUITY ANGLES

4.3.2 Ballistic Limit Equation.

The V_{50} equation determines the velocity at which a penetration will initially occur. While the classic definition of this parameter is probabilistic, this implementation is not strictly probabilistic. Classically, V_{50} is defined as the velocity where there is a 50% (P=0.5) probability of penetration taking place. Inspection of equation 21 shows that V_{50}, as implemented in the penetration equations, is not probabilistic. For impact velocities less than V_{50}, no penetration is predicted, and for impact velocities greater than V_{50}, penetration is predicted. The concept of penetration is also important; throughout this analysis any impact in which the fragment had no positive residual velocity is considered as not penetrating. There are many other definitions for penetration with some requiring only light to pass through the target for a penetration to be declared.

The UEDDAM code uses the ballistic limit equation developed from an equation used to describe the energy absorption capability for homogeneous metallic material [1]. This equation has yielded more accurate results in previous testing, including the effects of complex structures [4]. The ballistic limit equation used in this analysis is defined as

$$V_{50} = \sqrt{\frac{2 \cdot L \cdot G_d \cdot t^2}{m \cdot \cos^2(\theta)}} \tag{3}$$

where (in System International (SI) units)

L = Presented area perimeter (m)
G_d = Dynamic shear modulus (Pa)
t = Target thickness (m)
m = Mass of fragment (kg)

θ = Obliquity (degrees)
V_{50} = Velocity for ballistic limit (m/s)

This equation is colloquially known as the FAA Energy Equation, from its legacy of having been described in previous FAA documents [1], which refer to it as the energy absorption equation. The development of the energy absorption equation into the V_{50} used in the UEDDAM is shown below. This equation is stated in reference 1 exactly as follows:

$$E_A = \frac{L \cdot T \cdot t^2}{12 \cdot \cos^2(\theta)} \tag{4}$$

where

E_A = Absorption energy (ft-lbs)
L = Presented area perimeter (in.)
t = Target thickness (in.)
T = Dynamic shear modulus (lbf/in^2)
θ = Obliquity (degrees)

For the application of this equation within reference 1, it was further solved for t, to determine the required thickness of armor that would contain a fragment. In this form, the equation looks as follows:

$$t = \sqrt{\frac{E_A \cdot (12 \cdot \cos^2(\theta))}{L \cdot T}} \tag{5}$$

The absorption energy term (E_A) is the kinetic energy (KE) of the impacting fragment and can, thus, be expanded as

$$E_A = \tfrac{1}{2} \cdot m \cdot V^2 \tag{6}$$

where

m = Mass of fragment (lbm)
V = Fragment velocity (ft/s)

Substituting the absorption energy term into equation 5 and solving for V yields

$$V = \sqrt{\frac{2 \cdot L \cdot T \cdot t^2}{m \cdot (12 \cdot \cos^2(\theta))}} \tag{7}$$

In this form, the equation states the ballistic limit of the material. Converting all the variables into SI units, removing the unit conversion factor in the denominator (12 inches per foot), and restating the dynamic shear modulus (T) as G_d, yields equation 3.

The exact origin of the FAA Energy Equation (equation 4), as described in reference 1, is not fully known. However, the form of the equation indicates that it may have been derived from a simple physics model for shear energy required to plug a metal with a circular cylinder. A common reference for engineers, "Mark's Handbook for Mechanical Engineers," provides the following formula for calculating the force required to punch a round hole in a sheet of metal [5].

$$P = \pi \cdot d \cdot t \cdot s \tag{8}$$

where

π = a constant
d = diameter of plug (in.)
t = thickness of material (in.)
s = resistance to shearing (lbf/in^2)
P = force required to plug the metal (lbf)

The V_{50} is the velocity where 50% of the impacts, for a specific set of conditions, will penetrate. This value is strictly probabilistic; however, it may be assumed that a good approximation is to compute the minimum velocity required to create a plug in the target material. This is done by calculating the work done during the formation of a hole due to plugging. The formation of a cylindrical plug can be modeled as shown in figure 13.

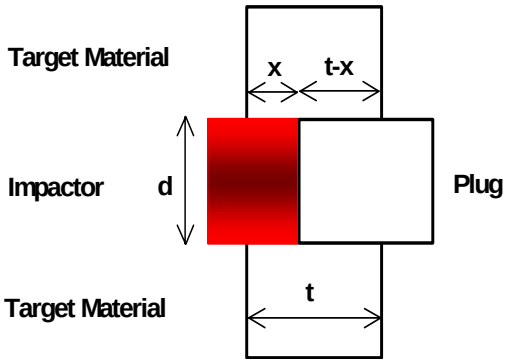


FIGURE 13. INTEGRATION RANGE FOR CYLINDRICAL PLUGGING MODEL

The work done is described as follows:

$$W = \int_0^t P(x)dx \tag{9}$$

Applying this to the formation of a cylindrical plug yields, where the region over which the shearing force acts is defined as t-x

$$W = \int_0^t L \cdot s \cdot (t - x)dx \tag{10}$$

where

$$L = \pi \cdot d$$

The integration formula applied to equation 10 is as follows [6].

$$\int (a + bx) dx = \frac{(a + bx)^{n+1}}{(n+1)b}; n \neq -1 \tag{11}$$

where

$$a = t$$
$$b = -1$$
$$n = 1$$

Thus, solving over the integral from 0 to t yields

$$W = L \cdot s \frac{t^2}{2} \tag{12}$$

The KE at impact is given by

$$K_e = \frac{1}{2} m \cdot V^2 \tag{13}$$

Assuming the normal component of impact velocity to be the only source of KE for plugging

$$V_n = V \cdot \cos(\theta) \tag{14}$$

where

θ = impact obliquity (degrees)

then

$$K_e = \frac{1}{2} m \cdot (V \cdot \cos(\theta))^2 \tag{15}$$

Equating the impact velocity to the work required to shear a plug

$$K_e = W \tag{16}$$

$$\frac{1}{2} m \cdot (V_{50} \cdot \cos(\theta))^2 = L \cdot s \frac{t^2}{2} \tag{17}$$

Then, solving for the velocity (V)

$$V_{50} = \sqrt{\frac{L \cdot s \cdot t^2}{m \cdot \cos^2(\theta)}} \tag{18}$$

Compare this to the FAA energy equation form below

$$V_{50} = \sqrt{\frac{2 \cdot L \cdot G_d \cdot t^2}{m \cdot \cos^2(\theta)}} \tag{19}$$

This implies that

$$s = 2 \cdot G_d \tag{20}$$

This derivation shows that the V_{50} equation probably originated from the formula for calculating the force required to punch a round hole in a sheet of metal. However, there is a slight difference, by the factor of 2 in the numerator. The discrepancy in equation 20 is not as important as it may seem. Reference 1 states that the dynamic shear modulus was determined empirically and the factor of 2 may have been introduced as a result of test data. Unfortunately, the method by which the dynamic shear modulus was obtained was not documented in reference 1.

Table 5 shows a comparison of known G_d and resistance to shearing (R_s) values from references 1 and 5, respectively. These values show only a very minimal correlation. However, these disparities may be attributed to the differences of impacting projectiles into panels that are attached on their edges, as opposed to punching a supported plate.

TABLE 5. COMPARISON OF MATERIAL CONSTANTS

Material	Dynamic Shear Modulus (G_d) (MPa)	Resistance to Shearing (R_s) (MPa)
Aluminum*	210	
Aluminum, 6S		103
Aluminum, 2S		69
Stainless Steel*	1300	
Stainless Steel (unspecified alloy)		393
Steel 0.10C		248
Steel 1.00C		793
Titanium*	996	

*Unspecified alloy from reference 1.

The physics-based origin of the V_{50} equation indicates that the G_d is a misnomer. This empirically derived parameter is more appropriately described as a shear constant. Henceforth, within this report the empirical constant within the V_{50} equation shall be stated as the C_s.

4.3.3 Residual Velocity Equation.

The residual velocity equation calculates the velocity of the fragment after a penetration has occurred. The equation used within UEDDAM was developed by the JTCG/ME to provide analysis tools to describe the impacts of antiaircraft artillery projectiles and shrapnel fragments from high explosive rounds. The penetration equations contained within reference 7 are in numerous forms. These different forms take into account the projectile characteristics and penetration mode. Previous testing has determined that optimal predictions for engine fan blade fragments can be obtained using the JTCG/ME residual velocity equation for blunt objects penetrating in a plugging mode. This equation is defined as

$$V_r = \frac{\sqrt{V_i^2 - V_{50}^2}}{1 + \frac{\rho \cdot A_p \cdot t}{m \cdot \cos(\theta)}} \tag{21}$$

where

θ = Obliquity (degrees)
ρ = Target material density (kg/m^3)
A_p = Presented area (m^2)
m = Mass of fragment (kg)
t = Target thickness (m)
V_i = Impact velocity (m/s)
V_r = Residual velocity (m/s)
V_{50} = Velocity for ballistic limit (m/s)

It is important to note that this equation is based on empirical data and is dependent upon using the correct SI units. The residual velocity equation has a mathematical limitation that is of practical importance. An imaginary result occurs when the V_{50} is greater than the impact velocity. When analyzing test data, this can occur, and the data point is not analyzable even though it is otherwise a valid data point.

4.4 SHEAR COEFFICIENT METHODOLOGY.

The penetration test data were used to determine the C_s for each material tested that would produce the best agreement between the actual and predicted residual velocities. The process used was multifold and required a computation of the root mean squared (rms) error for the correlation factors (Q factor), the simple percent error in residual velocities, and a measure of conservatism. An Excel spreadsheet was created that solved the penetration equations for all the impact data and then determined an rms error for the Q factors. The correlation factor, Q, is defined as

$$V_r = 1 - \frac{(V_{r,Test} - V_{r,Predicted})}{V_i} \tag{22}$$

where

V_i = Test impact velocity (m/s)
$V_{r,\ Predicted}$ = Penetration equation prediction for residual velocity (m/s)
$V_{r,\ Test}$ = Test residual velocity (m/s)

This correlation factor describes the square of the difference between measured test residual velocities and predicted residual velocities, offset to a scale of 1, and normalized by the initial velocity. This equation produces values between 0 and 2, where a value < 1 represents an under prediction and >1 an overprediction. Consequently, a value of 1 describes an accurate prediction. For each material, the correlation factor is plotted with respect to shot number. Since Q is a function of V_r, only test shots where a penetration occurred are plotted.

The rms error is defined as

$$E = \sqrt{\sum_{k=1}^{n} \frac{\left(\frac{(V_{r,Test} - V_{r,Predicted})}{V_i} \right)^2}{n}} \tag{23}$$

where

E = Prediction error
n = Number of test shots
V_i = Test impact velocity (m/s)
$V_{r,\ Predicted}$ = Penetration equation prediction for residual velocity (m/s)
$V_{r,\ Test}$ = Test residual velocity (m/s)

The shear constant was varied with the goal of having the Q factors equal unity. This process was automated with the Solver function in Excel. Any optimizer solution must be checked for local minima conditions since they can lead to false solutions. After a solution was found, the C_s was varied manually to explore the region for false minima. The percent error in residual velocities and the conservatism measure provided indications of the goodness of the solution.

When the V_r was lower than the V_{50}, the C_s became unsolvable and then dropped out of the running due to imaginary results. This is not allowed and was carefully monitored. The plots of the Q factors showed this effect graphically and immediately. A true/false measure of conservatism was computed to indicate that the C_s was likely to estimate a higher residual velocity than actual. The average of the conservatism values would vary from 0 to 1, with 1 being nonconservative. A value of 0.25 was considered acceptable as the upper limit of conservatism. In this manner, all the data were used to empirically locate the best C_s for the material being evaluated.

5. RESULTS.

The results presented in this section are in a condensed form, with the complete data contained in appendix B. The condensed test data was separated into two tables and one plot for each material evaluated under this test. One table contains the static test data: shot number, fragment mass, fragment dimensions, and panel thickness. The other data table contains the dynamic test parameters, combining the test data with the penetration equation predictions, and compares the two values via a correlation factor (prediction accuracy).

Fragment dimensions noted in the results are mean values and not the actual sizes. This approximation was necessary because the penetration equations modeled square and rectangular objects only. The use of fragments cut in horizontal sections from actual aircraft engine fan blades meant that the test fragments were mostly trapezoidal in shape. The dimensions listed in the results are the mean of the opposing sides (e.g., length=$[l_1 + l_2]/2$ and width=$[w_1 + w_2]/2$).

For the purposes of this test, the three modes of penetration are defined in the results: penetration, partial penetration, and a nonpenetration condition. A penetration describes the result of the fragment passing completely through the target material, from where a residual velocity can be determined. Partial penetrations occur when the target material is pierced and the fragment penetrates, but either does not continue all the way through or only a piece of it does. No residual velocities are determined from this mode of penetration. A nonpenetration condition is when the fragment has not passed through the material, even though the target material may be pierced.

5.1 GENERALIZED COMPOSITE.

Test data was successfully obtained from 26 of the 29 panels. Loss of test data occurred on only three shots (shots 31, 32, and 45), due to camera/lighting timing errors (shot 32) and camera malfunctions (shots 31 and 45). All composite panel test shots had complete fragment penetration. The analysis served to determine the C_s for composite materials. Fragment masses and dimensional parameters with respect to shot number are described in table 6. It should be noted that the thickness stated in the right-hand column of this table refers only to the thickness of the graphite layers, for reasons that are discussed later.

The test plan stated that for each fragment size, orientation, and panel thickness, testing would be performed at three velocities: 500 ft/s, 650 ft/s, and 800 ft/s. However, following the first few panels, it became obvious that very little energy was being removed from the fragment during penetration. This became a concern with regards to the accuracy of the velocity data from the film analysis in that the delta velocity was so small it may be within in the accuracy of the film analysis method. Subsequently, test velocities were modified to be within the 200 ft/s to 450 ft/s region. It was not possible to achieve velocities below 200 ft/s due to limitations of the gas gun. Actual test initial and residual velocities are listed in table 7.

TABLE 6. COMPOSITE PANEL IMPACT—PHYSICAL DATA

Shot Number	Fragment Mass *m* (gm)	Fragment Length (x axis) (in.)	Fragment Width (z axis) (in.)	Plate Thickness *t* (in.)
25	244	7.688	2.938	0.060
26	244	7.688	2.938	0.060
27	244	7.688	2.938	0.060
30	244	7.688	2.938	0.060
33	244	7.688	2.938	0.060
34	244	7.688	2.938	0.060
35	244	7.688	2.938	0.060
36	244	7.688	2.938	0.060
38	244	7.688	2.938	0.060
39	244	7.688	2.938	0.060
40	244	7.688	2.938	0.060
41	244	7.688	2.938	0.060
42	244	7.688	2.938	0.060
43	650	7.750	7.375	0.060
44	650	7.750	7.375	0.060
47	650	7.750	7.375	0.060
48	650	7.750	7.375	0.060
49	650	7.750	7.375	0.060
50	650	7.750	7.375	0.060
51	650	7.750	7.375	0.060
52	650	7.750	7.375	0.060
53	650	7.750	7.375	0.060
54	650	7.750	7.375	0.060
55	650	7.750	7.375	0.060
56	244	7.688	2.938	0.060
57	244	7.688	2.938	0.060

The initial posttest analysis did not show any correlation between the penetration equations and test data. Solving for the C_s yielded no result if all the composite honeycomb thickness was considered. Three different results were obtained if each panel thickness was solved for individually. With the generalized composite lay-up used in testing, density decreased with overall thickness (graphite layers and honeycomb). Figure 14 shows a plot of density with respect to panel honeycomb thickness.

Further analysis determined that the honeycomb section of the composite panel contributed very little to the ballistic tolerance of the panel. Consequently, the analysis was performed with the thickness parameter in the penetration equations, *t*, input as that of the graphite layers only (figure 15). For all panels tested, the mean thickness of the graphite layers was 0.060″, six layers of woven 0.008″ thick graphite, with the additional 0.002″ accounted for in the resin. The density of the graphite layers only was determined to be 1545 kg/m^3.

TABLE 7. COMPOSITE PANEL IMPACT—DYNAMIC DATA

Shot Number	Impact Velocity V_i (ft/s)	Residual Velocity V_r (ft/s)	Presented Area A_p (in^2)	Perimeter of Presented Area L (in.)	Ballistic Limit V_{50} (ft/s)	Residual Velocity Estimate $V_r^{\sim}$ (ft/s)	Correlation Factor Q $1-(V_r-V_r^{\sim})/V$
25	512	441	10.0	12.8	129.5	466.4	1.05
26	383	311	14.1	15.7	143.1	326.6	1.04
27	214	166	5.4	9.8	112.9	176.3	1.05
30	223	143	18.2	18.9	157.1	142.5	1.00
33	364	308	3.1	13.7	133.6	332.1	1.07
34	342	299	5.7	10.2	115.6	310.6	1.03
35	154	88	14.4	19.1	158.2	≈0*	-
36	165	99	15.2	16.3	145.8	70.3	0.82
38	254	155	20.1	20.6	164.1	172.8	1.07
39	473	409	6.1	10.5	117.3	441.4	1.07
40	470	409	10.0	12.7	128.8	425.6	1.04
41	308	270	5.2	10.2	115.7	276.0	1.02
42	304	242	10.3	12.9	129.8	258.0	1.05
43	381	303	25.7	22.9	105.9	345.3	1.11
44	307	225	51.4	28.7	118.6	253.0	1.09
47	406	358	15.1	18.9	96.3	381.4	1.06
48	248	193	55.6	29.8	121.0	191.4	0.99
49	240	196	42.5	26.4	113.7	192.0	0.98
50	383	296	43.7	26.6	114.3	332.0	1.09
51	327	237	46.2	27.3	115.7	276.3	1.12
52	260	217	3.5	18.9	96.2	239.5	1.09
53	351	255	53.0	29.1	119.5	293.3	1.11
54	311	229	45.1	27.2	115.6	261.7	1.11
55	237	111	56.7	30.1	121.5	179.8	1.29
56	270	185	18.3	18.4	154.9	198.6	1.05
57	269	227	7.4	11.7	123.5	228.7	1.01

A C_s value of 251 MPa for the generalized composite panel was determined as optimal from the 26 test data points. Figure 16 shows the prediction accuracy of the penetration equations in determining the residual velocity when using the aforementioned C_s (251 MPa) and the graphite thickness only.

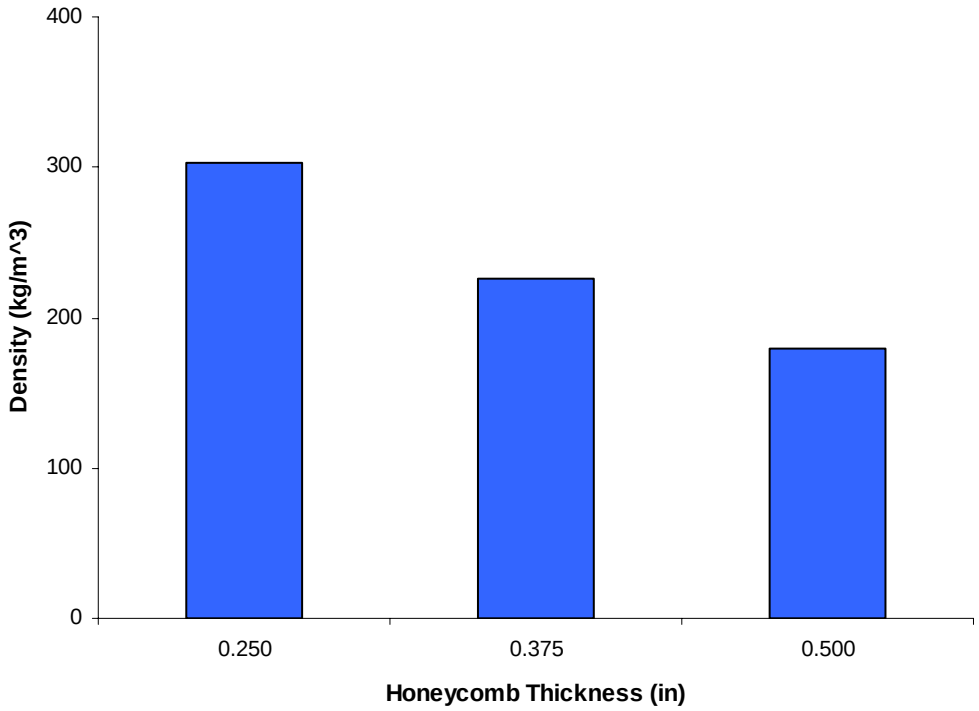


FIGURE 14. GENERALIZED COMPOSITE PANEL DENSITY WITH RESPECT TO THICKNESS

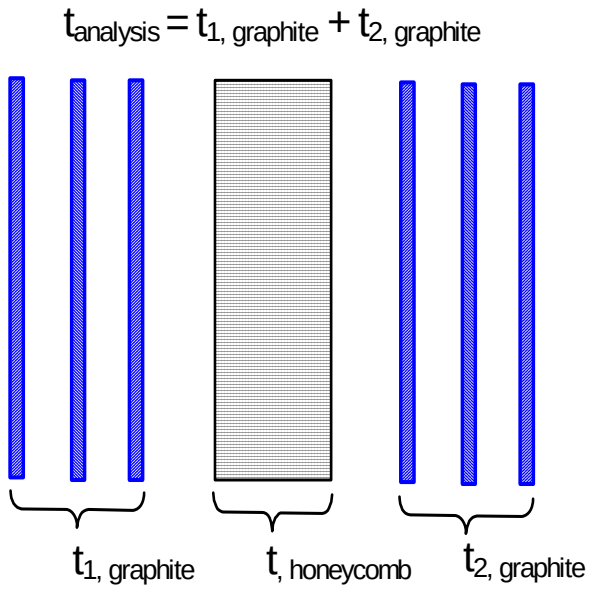


FIGURE 15. COMPOSITE PANEL BALLISTIC ANALYSIS THICKNESS

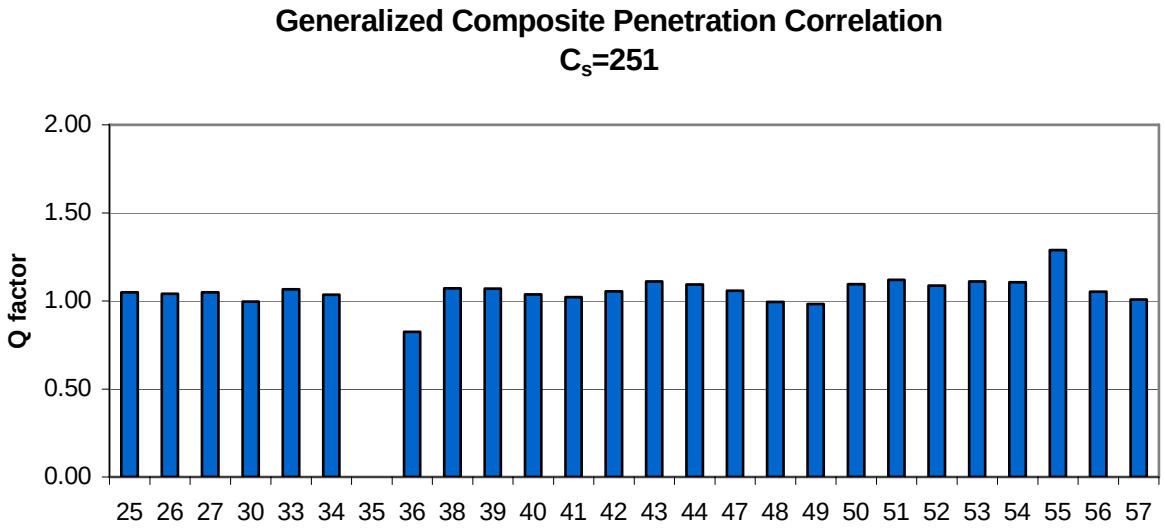


FIGURE 16. EXPERIMENTAL CORRELATION FOR COMPOSITE PANELS

The damage to the composite panels due to fragment impacts was usually considerable, especially in cases where the presented area of the fragment was large. For most impacts during this test, the damaged area exceeded the area where impact occurred. This was in contrast to the damage seen with the metal panels. Figure 17 shows an example of very minor damage (localized to the impact area) caused by a 3″ by 8″ fragment with a small A_p. However, in most impacts, the damage propagated through large areas of the panel, as shown in figure 18. In both examples, the observed damage can be compared to a single-sided petaling case in a metal.



FIGURE 17. MINOR COMPOSITE PANEL DAMAGE



FIGURE 18. MAJOR COMPOSITE PANEL DAMAGE

5.2 2024-T351 ALUMINUM.

A total of fifteen 2024-T351 aluminum panels were tested under Phase II (Component Shielding Materials) of this test. Only one shot failed to produce usable data (shot 6) due to a HS camera failure. Of the 14 successfully instrumented tests, 10 impacts did not penetrate. Early sabot design and setup problems produced higher than desired presented areas (shots 3-10), resulting in no penetration. However, these high A_p impacts are all valuable data points because they correlated with the predicted result from the V_{50} in that no penetration occurred below the ballistic limit velocity for a given fragment orientation. Table 8 lists the fragment masses and dimensional data for each shot within the 2024-T351 aluminum test series.

TABLE 8. 2024-T351 ALUMINUM PANEL IMPACT—PHYSICAL DATA

Shot Number	Fragment Length Average (x axis) (in.)	Fragment Width Average (z axis) (in.)	Fragment Mass *m* (gm)	Plate Thickness *t* (in.)
3	7.625	7.563	772	0.250
4	7.625	7.563	772	0.250
5	7.625	7.563	772	0.250
7	7.625	7.563	770	0.250
8	7.625	7.563	770	0.375
9	7.125	7.938	748	0.375
10	7.125	7.938	748	0.375
23	7.625	7.750	715	0.375
24	7.125	7.938	748	0.375
64	7.750	7.375	741	0.250
65	7.750	7.375	741	0.250
66	7.750	7.375	650	0.250
67	7.750	7.375	679	0.250
68	7.750	7.375	679	0.250

Impact velocities were selected to bound the V_{50}. Preshot ballistic limit predictions were calculated using the previously accepted G_d value of 210 MPa [1]. Actual test impact data, including velocities and blade orientation are shown in table 9.

TABLE 9. 2024-T351 ALUMINUM PANEL IMPACT—DYNAMIC DATA

Shot Number	Impact Velocity V_i (ft/s)	Residual Velocity V_r (ft/s)	Presented Area A_p (in^2)	Perimeter of Presented Area L (in.)	Ballistic Limit V_{50} (ft/s)	Residual Velocity Estimate $V_r^{\sim}$ (ft/s)	Correlation Factor Q $1-(V_r-V_r^{\sim})/V$
3	553	0	57.7	30.4	489	140	1.25
4	541	0	56.1	30.0	486	131	1.24
5	368	0	42.3	26.3	456	≈0*	-
7	402	0	53.7	29.3	482	≈0*	-
8	499	0	3.8	16.1	536	≈0*	-
9	588	0	56.6	30.1	1017	≈0*	-
10	608	0	49.8	28.4	721	≈0*	-
23	603	229	5.7	17.0	571	172	0.91
24	554	0	22.0	21.6	629	≈0*	-
64	445	0	43.3	26.7	468	≈0*	-
65	469	0	37.2	24.9	452	79	1.17
66	563	207	31.6	23.4	468	202	0.99
67	536	339	3.7	16.8	388	349	1.02
68	511	283	12.3	18.7	409	254	0.94

*Cases where $V_{50} > V_i$ produce imaginary results from the penetration equation; the implication is that no penetration is predicted.

Data from the two previous tests were included in the analysis of the aluminum impacts such that the shear constant would be optimized for all thicknesses of material [3 and 4]. All the aluminum previous testing data were included. This brought 52 impacts into the analysis and provides a more representative C for impacts into aluminum aircraft structure. An optimal C_s of 276 MPa was determined. This value compared very favorably to the previously accepted dynamic shear modulus of 210 MPa. It should be noted here, for clarity, that the (C_s) and G_d are the same variable within the ballistic limit equation. However, this change in nomenclature is due to the analysis and improved understanding of the origin of this empirical parameter, now more appropriately defined as a constant than a modulus. Figure 19 shows the prediction accuracy of the penetration equations (C_s = 276 MPa) in determining the V_r. Figure 20 shows the blade fragment for shot 8, following the test, with the leading edge rolled and missing in places.

Considerable deformation and frangibility of the fragment were observed frequently during Phase II of testing, where the materials were of greater thickness than aircraft skins and stiffeners. The effect of fragment deformation was that the penetration equations had a tendency to overpredict the ballistic limit and residual velocity (i.e., penetration did not occur at velocities in excess of the ballistic limit). Fragment deformation and frangibility are complex and dynamic

processes that are not considered in either the ballistic limit (equation 4) or residual velocity equation (equation 21). When the leading edge of the blade curls upon impact, the A_p increases dynamically and, in some cases, causes the fragment to rotate and impact at a lower fragment angle (θ). Figure 21 illustrates this process (from shot 8), where the gouge in the panel is considerably wider than the thickness of the fragment's leading edge. In addition, this figure clearly shows the outline of the fragment when it rotated, creating a very large A_p. The result is that the condition of the impactor changes throughout the impact. The development and derivation of the penetration equations did not consider this phenomena [8].

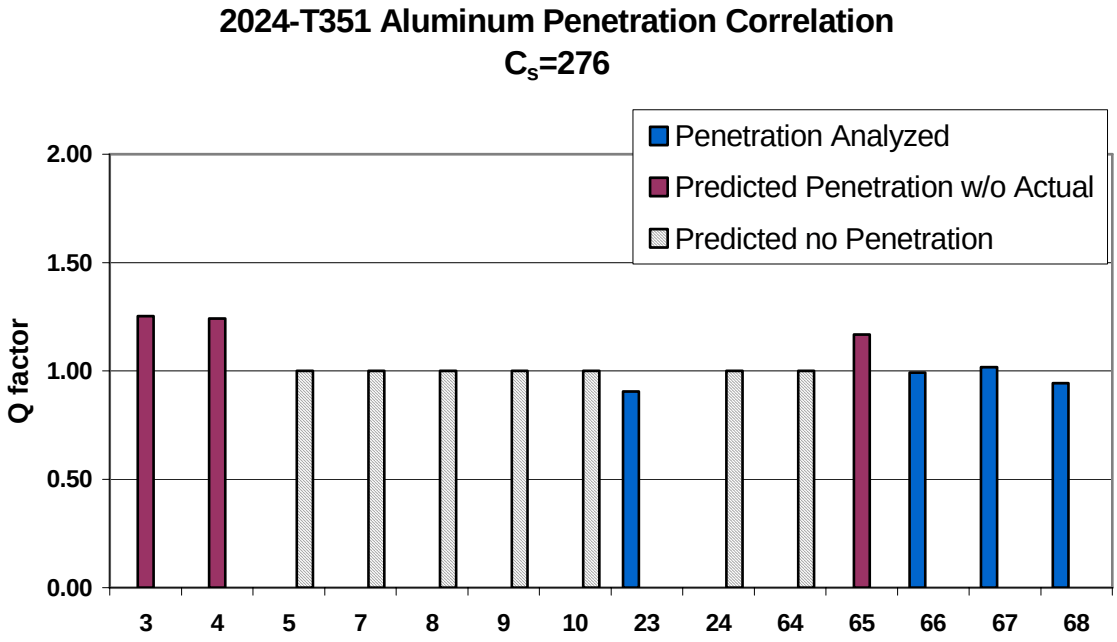


FIGURE 19. EXEPERIMENTAL CORRELATION FOR ALUMINUM PANELS



FIGURE 20. FRAGMENT DEFORMATION DUE TO IMPACT



FIGURE 21. PANEL DAMAGE DUE TO FRAGMENT DEFORMATION

Confidence has been achieved in the capability of the penetration equations to predict the V_{50} for 2024-T351 aluminum (C_s = 276 MPa). For the seven impacts where the penetration equations estimated no penetration would take place, none occurred (see figure 22).

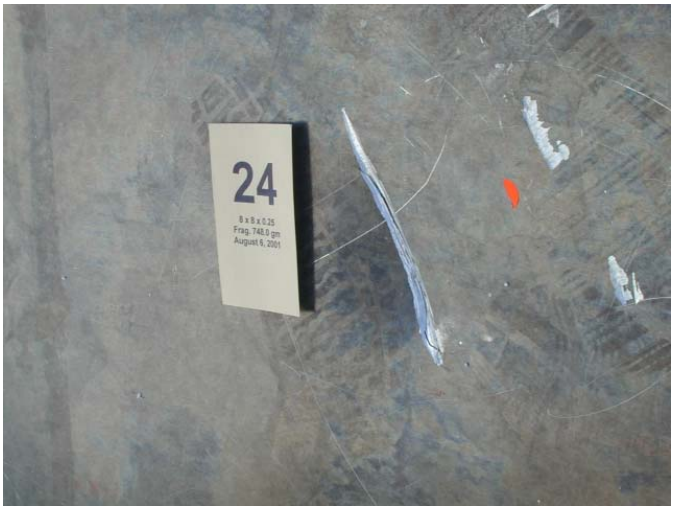


FIGURE 22. PANEL DAMAGE AT BALLISTIC LIMIT

5.3 Ti-6Al-4AV TITANIUM.

A total of 13 Ti-6Al-4V titanium panels were tested under the component shielding materials phase of this test. Data was successfully obtained from all shots. Camera failure occurred on two shots (shots 14 and 16); however, impact data was obtained from the digital HS cameras that were operating in an evaluation role. The fragment physical properties are listed in table 10.

TABLE 10. Ti-6Al-4V TITANIUM PANEL IMPACT—PHYSICAL DATA

Shot Number	Fragment Mass *m* (gm)	Fragment Length (x axis) (in.)	Fragment Width (z axis) (in.)	Plate Thickness *t* (in.)
Pre2	800.0	7.500	7.313	0.063
Pre3	767.0	7.625	7.563	0.063
Pre4	740.0	7.125	7.813	0.063
11.0	740.0	7.125	7.813	0.125
12.0	740.0	7.125	7.813	0.125
13.0	738.0	7.250	7.813	0.125
14.0	714.0	7.250	7.813	0.125
15.0	714.0	7.250	7.813	0.125
16.0	714.0	7.250	7.813	0.250
17.0	703.0	7.625	7.563	0.250
18.0	723.0	7.125	7.875	0.250
19.0	680.0	6.375	7.500	0.250
20.0	702.0	7.125	7.250	0.250
21.0	639.0	6.000	7.500	0.250
22.0	577.0	6.500	7.125	0.250

Except for the pretest shots (0.063″ thick material), all panels were tested with velocities in the region of the V_{50}. The selection of impact velocities was calculated via the penetration equations, using the previously described G_d for an unspecified alloy type titanium of 996 MPa. Impact data for each shot is listed in table 11.

Posttest analysis of the test data determined that an optimal C_s of 900 MPa provided the most accurate predictions for Ti-6Al-4V titanium. Figure 23 shows the prediction accuracy of the penetration equations (C_s = 900 MPa) in determining the residual velocity.

Significant fragment deformation and frangibility were observed with the impacts into the 0.125″ and 0.250″ thick Ti-6Al-4V material, causing some anomalies in the test data. Shots 20, 21, and 22 had fragment impact velocities at approximately twice the ballistic limit, but no penetration occurred. In shot 20, the fragment fractured upon impact (figure 24), piercing the material along the contact edge (see figure 25). In the consecutive shot (shot 21), the fragment was both fractured and deformed (figure 26), but failed to even pierce the material (figure 27). As mentioned previously, these modes of penetration (fragment deformation and frangibility) are not modeled by the penetration equations. However, two shots into the 0.250″ material did successfully penetrate (shots 16 and 17), thus verifying the credibility of the ballistic limit for this material and thickness. Only one shot (shot 15) into the 0.125″ material failed to penetrate.

Again, this fragment was impacted in excess of twice the ballistic limit velocity. Analysis of the HS film shows that the fragment had penetrated through to approximately one quarter of its length, before bouncing off.

TABLE 11. Ti-6Al-4V TITANIUM PANEL IMPACT—DYNAMIC DATA

Shot Number	Impact Velocity V_i (ft/s)	Residual Velocity V_r (ft/s)	Presented Area A_p (in^2)	Perimeter of Presented Area L (in.)	Ballistic Limit V_{50} (ft/s)	Residual Velocity Estimate $V_r^{\sim}$ (ft/s)	Correlation Factor Q $1-(V_r-V_r^{\sim})/V$
Pre2	647	442	47.3	27.7	≈0*	≈0*	-
Pre3	427	294	45.7	27.3	≈0*	≈0*	-
Pre4	309	246	5.0	18.6	209	474	1.05
11.0	426	155	4.8	18.3	212	286	0.98
12.0	406	212	3.9	16.7	178	244	0.99
13.0	379	8	21.7	21.0	350	229	1.17
14.0	341	0	4.9	16.9	335	218	1.01
15.0	365	0	4.7	16.8	376	33	1.07
16.0	723	211	3.9	17.6	184	233	1.68
17.0	780	269	3.8	16.2	342	120	1.33
18.0	501	0	26.1	41.4	328	435	1.31
19.0	495	0	41.4	26.0	677	351	1.10
20.0	748	8	3.6	15.6	≈0*	≈0*	-
21.0	781	0	3.7	33.1	≈0*	≈0*	-
22.0	871	0	3.6	30.5	665	311	1.40

*Cases where $V_{50} > V_i$ produce imaginary results from the penetration equation; the implication is that no penetration is predicted.

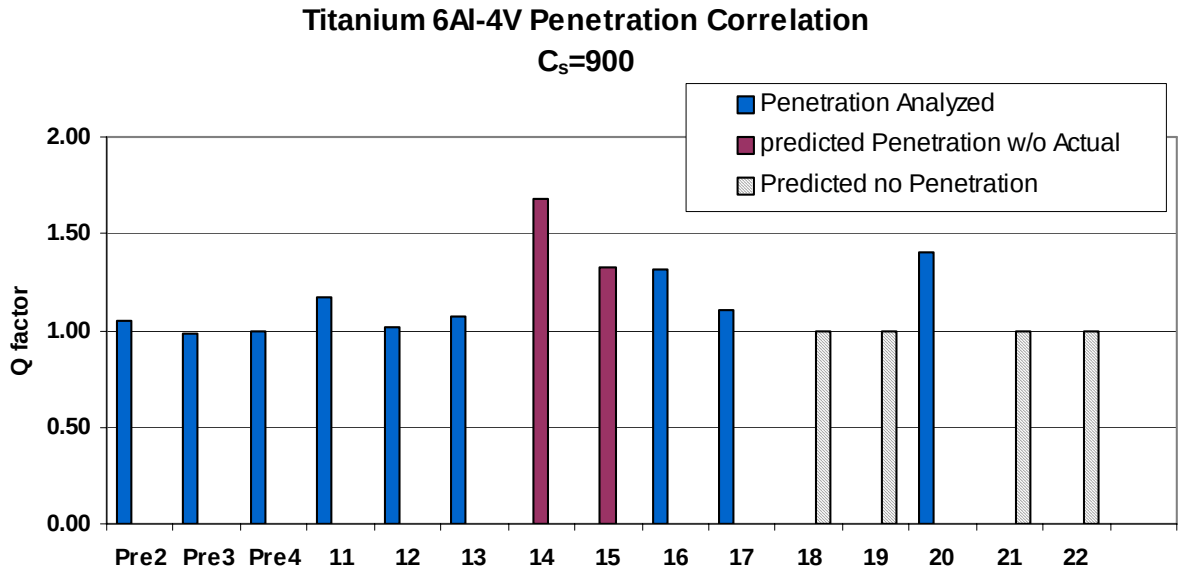


FIGURE 23. EXPERIMENTAL CORRELATION FOR Ti-6Al-4V TITANIUM PANELS



FIGURE 24. FRAGMENT BREAKUP FOR SHOT 20



FIGURE 25. PANEL DAMAGE FOR SHOT 20



FIGURE 26. FRAGEMENT DEFORMATION FOR SHOT 21



FIGURE 27. PANEL DAMAGE FOR SHOT 21

5.4 INCONEL 625 LCF.

The test series for the Inconel 625 LCF material consisted of six shots, resulting in four penetrations and two partial penetrations. Data was obtained successfully from all six shots. All six panels were 0.063″ thick. The fragment dimensions and masses are listed in table 12.

TABLE 12. INCONEL 625 LCF IMPACT—PHYSICAL DATA

Shot Number	Fragment Mass m (gm)	Fragment Length (x axis) (in.)	Fragment Width (z axis) (in.)	Plate Thickness t (in.)
58	650	7.750	7.375	0.063
59	650	7.750	7.375	0.063
60	650	7.750	7.375	0.063
61	650	7.750	7.375	0.063
62	650	7.750	7.375	0.063
63	741	7.750	7.375	0.063

Ballistic testing of this material, or any other superalloy, had never been performed at NAWC-WD before. Thus, the ballistic response of this material was unknown. To estimate an approximate V_{50} regime in which to test the Inconel panels, a C_s value of twice the G_d for the unspecified alloy titanium was used within the penetration equations ($C_s \approx 1700$ MPa) [1]. This assumption provided a reasonable degree of prediction accuracy. Table 13 lists the dynamic shot data for the Inconel tests.

TABLE 13. INCONEL 625 LCF IMPACT—DYNAMIC DATA

Shot Number	Impact Velocity V_i (ft/s)	Residual Velocity V_r (ft/s)	Presented Area A_p (in^2)	Perimeter of Presented Area L (in.)	Ballistic Limit V_{50} (ft/s)	Residual Velocity Estimate $V_r^{\sim}$ (ft/s)	Correlation Factor Q $1-(V_r-V_r^{\sim})/V$
58	418	308	23.67	21.29	235	263	0.89
59	434	0	42.55	26.30	261	221	1.51
60	458	298	22.20	21.28	235	303	1.01
61	424	294	3.68	16.06	204	355	1.14
62	366	253	3.57	18.31	218	281	1.08
63	340	0	36.27	24.73	237	171	1.50

*Cases where $V_{50} > V_i$ produce imaginary results from the penetration equation; the implication is that no penetration is predicted.

Analysis of the test data determined a C_s value of 1200 MPa from the six test shots. The prediction accuracy of the penetration equations using this value for C_s is shown in figure 28.

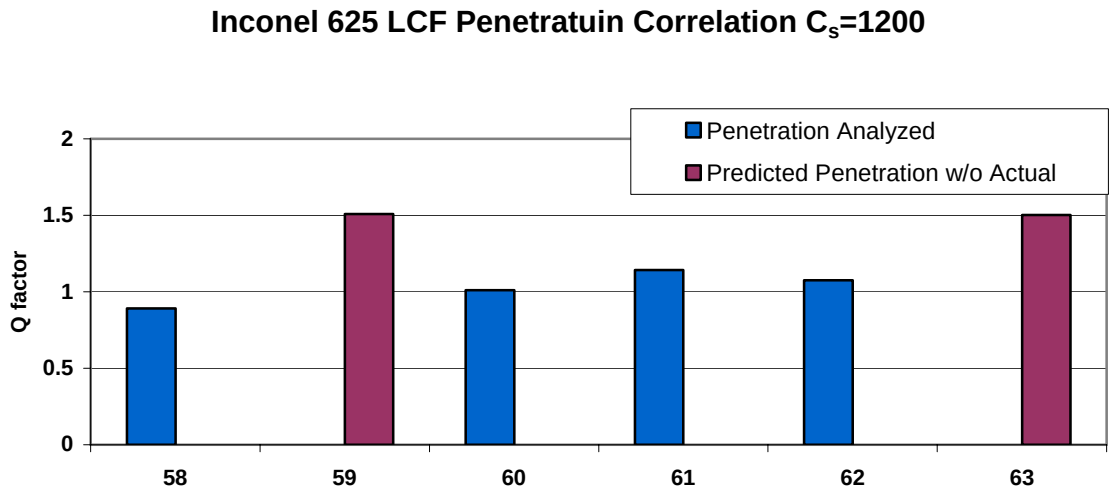


FIGURE 28. EXPERIMENTAL CORRELATION FOR INCONEL 625 LCF PANELS

5.5 SHEAR PARAMETER DISCUSSION.

During the course of the data analysis, an improved comprehension of the ballistic limit equation (FAA Energy Equation) was attained. This equation is used within reference 1, but the original equation is never defined. The variables and inputs for this equation are rather self-explanatory, with the exception of the parameter denoted as the G_d. From the previous discussion on the ballistic limit, it was illustrated that this equation compares well to the simple physics model for shear energy required to shear a circular plug in a metal plate. The manner in which the material constant is contained within the FAA Energy Equation implies that it is more appropriate to term this parameter a C_s rather than a G_d. The term dynamic shear modulus is typically applied to engineering problems involving earth landslides and seldom to metals. Henceforth, when discussing this parameter within the results section of this report, it is referred to as the C_s. If the value for the material constant predates this report, then it is referred to as the G_d.

Another factor that was noted in the data analysis for this test was the approximate relationship between G_d, ultimate shear strength (F_{su}), and resistance to shearing (R_s). Table 14 lists these properties for comparison. The first two columns list the values for the former material constant (G_d) and then the values obtained from the current test series, now known as the C_s. In the last two columns, the resistance to R_s and F_{su} values are listed to illustrate that they are all closely related but not the same. This relationship indicates that for untested materials, a first-cut rough estimate could be obtained by using the R_s or F_{su} values for the C_s in the penetration equations.

TABLE 14. COMPARISON OF MATERIAL PROPERTIES

Material	Shear Constant (C_s) (MPa)	Dynamic Shear Modulus (G_d) [1] (MPa)	Resistance to Shearing (R_s) [5] (MPa)	Ultimate Shear Strength (F_{su}) [9] (MPa)
2024-T351 Aluminum	276			283
Aluminum (unspecified alloy)		210		
Aluminum, 6S			103	193
Aluminum, 2S			69	
Stainless Steel, ANSI-321		1300		655
Stainless Steel (unspecified alloy)			393	
Steel 0.10C			248	
Steel 1.00C			793	
Titanium (unspecified alloy)		996		
Ti-6Al-4V	900			689
Inconel 625				562
Inconel 625 LCF	1200			

The data listed in table 14 is presented to aid future work if a ballistic prediction is required for an untested material. It is worth noting the following relations are loosely indicated for the aluminum and steel data in this table.

$$G_d \approx 2 \cdot R_s \tag{24}$$

and

$$C_s \approx G_d \tag{25}$$

6. CONCLUSION.

Testing was conducted on four materials for the purposes of supporting the Uncontained Engine Debris Damage Analysis Model (UEDDAM) analysis tool: 2024-T351 aluminum, Ti-6Al-4V titanium, Inconel® 625 low-cycle fatigue (LCF), and a generalized composite. Analysis of the impact data provided an empirical database to determine the material property and shear constant (C_s), which are used to define the ballistic performance of the target material within the penetration equations. Optimal C_s were obtained from the test data for all four materials investigated. Additionally, this test also refined the value of the shear constant to reference a specific alloy type for each material. The recommended values for the C_s, based on all testing performed to-date, are listed in table 15.

A more comprehensive understanding of the penetration equations has been achieved via this testing and the subsequent data analysis. The material constant used within the ballistic limit equation was formerly known as the dynamic shear modulus [1]. Following the comparative analysis of the FAA Energy Equation to the physics-based equation for the formation of a cylindrical plug, it was shown to be more terminologically accurate to describe this material property as the C_s. In addition, some correlation has been made between the C_s, resistance to shearing (R_s), and the ultimate shear strength (F_{su}) of a material. This correlation can serve as a guideline for applying the penetration equations to materials that have not been previously tested, if initial estimates are all that is required. However, if a more accurate prediction is required, then a series of test shots should be performed to characterize the material.

TABLE 15. MATERIAL SHEAR STRENGTH (C_s) SUMMARY*

Material Type	Shear Constant (C_s) (MPa)
2024-T351 aluminum	276
Ti-6Al-4V titanium	900
Inconel 625 LCF	1200
Generalized composite	251
Stainless Steel 321 in annealed condition [1]	1300

7. RECOMMENDATIONS.

This test has provided data to both update and support the prediction capabilities of the penetration equations. Two new materials have been characterized for their ballistic performance to uncontained engine debris (generalized composite and Inconel 625 LCF). In addition, the relationship between the penetration equation's material constant (formerly the dynamic shear modulus) and the material ultimate shear strength has been observed. This correlation may allow the penetration equations to be used for predictions of other metals. However, this relationship is not expected to hold true for nonmetals. Further testing could be used to investigate complex composites and plastics, such as Lexan®.

Future ballistic testing to characterize materials should emphasize a greater number of shots designed to penetrate the material. The purpose is to use as many data points as possible in the analysis to determine the material C_s. Test shots where the V_i is less than the V_{50} result in imaginary numbers within the Joint Technical Coordinating Group on Munitions Effectiveness residual velocity equation.

* These values are empirically derived from test data and are coded into UEDDAM 2.0.4 Refer to the latest UEDDAM users manual for updates.

With the increasing size of turbine engines, blade fragments larger than 8″ by 8″ (0.75 lb) and disk segments larger than 3 lb should be investigated. It is possible that the shear constants found here may not apply to the very massive debris that is possible from the newer engines.

8. REFERENCES.

1. Gunderson, C., "Study to Improve Airframe Turbine Engine Rotor Blade Containment," McDonnell Douglas Corp, FAA report RD-77-44, July 1977.

2. Manchor, J. and Frankenberger, C., "Engine Debris Penetration Testing," FAA report, DOT/FAA/AR-99/19, June 1999.

3. Lundin, S., "Engine Debris Fuselage Penetration Testing Phase I," FAA report, DOT/FAA/AR-01/27, September 1999.

4. Lundin, S., "Engine Debris Fuselage Penetration Testing Phase II," FAA report, DOT/FAA/AR-01/27, II, August 2002.

5. Avallone, E. and Baumeister, T., "Marks' Standard Handbook for Mechanical Engineers," McGraw-Hill, Tenth Edition, 1996.

6. Shelby, S., "CRC Standard Mathematical Tables," Ninth Edition, The Chemical Rubber Co., 1971.

7. "Penetration Equations Handbook for Kinetic-Energy Penetrators (U)," Joint Technical Coordinating Group for Munitions Effectiveness (Anti-Air), 61 JTCG/ME-77-16, Revision 1, 15 October 1985.

8. "The Resistance of Various Metallic Materials to Perforation by Steel Fragments," Ballistic Analysis Laboratory, Johns-Hopkins University, Baltimore, MD, BAL, THOR TR No. 51, Declassified, April 1963.

9. Military Handbook, "Metallic Materials and Elements for Aerospace Vehicle Structures," MIL-HNDBK-5H, 1 December 1998.

APPENDIX A—DETAILED TEST PLAN

DETAILED TEST PLAN

FAA Penetration Equation Evaluation for Advanced Aircraft Materials

PREPARED BY:

Richard Mueller
Project Engineer
Code 418300D

ACCEPTED BY PERFORMING ORG.:

Jay Kovar
Head, Weapons Survivability Lab
Code 418300D

REVIEWED BY:

Charles Frankenberger
Project Engineer
Code 418300D

CONCURRED BY:

A. J. Wearner
Head, Systems Vulnerability Branch
Code 418300D

CONCURRED BY:

Mike Gallagher
WSL Firing Officer
Code 418300D

APPROVED BY:

Richard (Tim) Horton
Head, Survivability Division
Code 418000D

CONTENTS

LIST OF FIGURES ii

LIST OF TABLES ii

1. SCOPE 1

2. BACKGROUND 1

3. TEST OBJECTIVE 1

4. APPROACH 2

4.1. Test Article Description 2

4.2. Test Matrix 3

4.2.1. Systems Check-Out Tests 4

4.2.2. Composite Panel Tests 4

4.2.3. Aluminum Panel Tests 5

4.2.4. Titanium Panels Tests 7

4.2.5. Inconel Panel Tests 9

4.3. PRE-TEST PREDICTIONS 10

4.4. PRE-TEST PREPARATION AND SETUP 10

4.4.1. Test Specimen Preparation 10

4.4.2. Test Facility Requirements 11

4.4.3. Test Pad Setup 12

4.5. DATA REQUIREMENTS 13

4.5.1. Instrumentation 13

4.5.2. Optical and Audio Records 19

4.6. TEST PROCEDURE 20

5. TEST CONSTRAINTS 20

5.1. ENVIRONMENTAL 20

5.2. SAFETY AND SECURITY 20

5.3. LOGISTICAL 21

6. DOCUMENTATION 21

APPENDIX A 22

APPENDIX B 25

APPENDIX C 28

LIST OF FIGURES

Figure 1: Composite Panel Lay-up 3
Figure 2: Predicted V_{50} for 0.250" Aluminum 6
Figure 3: Predicted V_{50} for 0.375" Aluminum 7
Figure 4: Predicted V_{50} for 0.125" Titanium 8
Figure 5: Predicted V_{50} for 0.250" Titanium 9
Figure 6: Complete Fan Blade Dimensions 11
Figure 7: Suggested Cutting Pattern for Fan Blades 11
Figure 8: Test Pad Setup 13
Figure 9: Camera Setup Geometry 16
Figure 10: Camera Setup Dimensions (24mm Focal Length Lens) 16
Figure 11: Background Board Setup 18
Figure 12: Test Pad Lighting Setup 19

LIST OF TABLES

Table 1: Metal Panel Materials List 3
Table 2: Systems Check-out Test Series 4
Table 3: Composite Panel Test Series 5
Table 4: Aluminum 2024-T3 Panel Test Series 7
Table 5: Titanium Ti-6AL-4V Panel Test Series 9
Table 6: Inconel® 625 LCF Panel Test Series 10
Table 7: High-Speed Film Setup Parameters 15
Table 8: FOV Width and Pictures per FOV Width 16
Table 9: Time Line for HS Cameras with Respect to Fire Signal 17
Table 10: Time Line for Flash Bulbs with Respect to Breakwire 17

1. SCOPE

This test is a continuation of the Naval Air Warfare Center, Weapons Division's (NAWCWD), Uncontained Engine Debris Damage Mitigation Program sponsored by the Federal Aviation Administration (FAA). In this phase of the program, the penetration characteristics of composite and fuel tank armor are to be investigated. The test data will be used to add capabilities to the empirical model and to validate, the penetration equations used within the Uncontained Engine Debris Damage Assessment Model (UEDDAM).

2. BACKGROUND

Uncontained engine debris events, although not very common, can cause severe damage to aircraft and can result in a loss of life. Improvements in engine design and manufacture can mitigate, but not prevent the occurrence of such failures, so aircraft must be designed to be able to minimize the effects of such damage. Engine debris damage mitigation features include: the placement of systems, their redundancy and separation, and the location of major aircraft structural components. Such aspects of the design must be determined in the early stages of an aircraft's development, for which the FAA and NAWCWD have embarked on a program to provide specialized tools for industry.

NAWCWD is currently involved with the Catastrophic Failure Prevention Program sponsored by the Federal Aviation Administration (FAA). The purpose of this effort is to develop an analytical tool to conduct commercial aircraft rotor burst assessments. The UEDDAM is a computer code based on the vulnerability assessment codes used by the Department of Defense (DoD). This code determines possible impact points on the aircraft structure from engine debris and then determines whether the fragment will penetrate the component or structure. Modeling of debris penetration is performed using a set of penetration equations based on those developed by the Joint Technical Coordinating Group for Munitions Effectiveness (JTCG/ME).

In an ongoing effort by NAWCWD to increase the validity of the UEDDAM code, testing has been conducted on actual aircraft nacelles, fuselage skins, components, and complex structures. This current phase of testing is designed to expand the methodology to include composite materials and new materials currently used in industry for fuel tank armor.

3. TEST OBJECTIVE

The objective of this test is to obtain data on the ballistic response of composite structures and shielding materials to engine fan blade and disk fragments. This data will be utilized to validate the penetration equations for materials already contained within the UEDDAM and to develop equation coefficients for new materials to further enhance the codes capability.

4. APPROACH

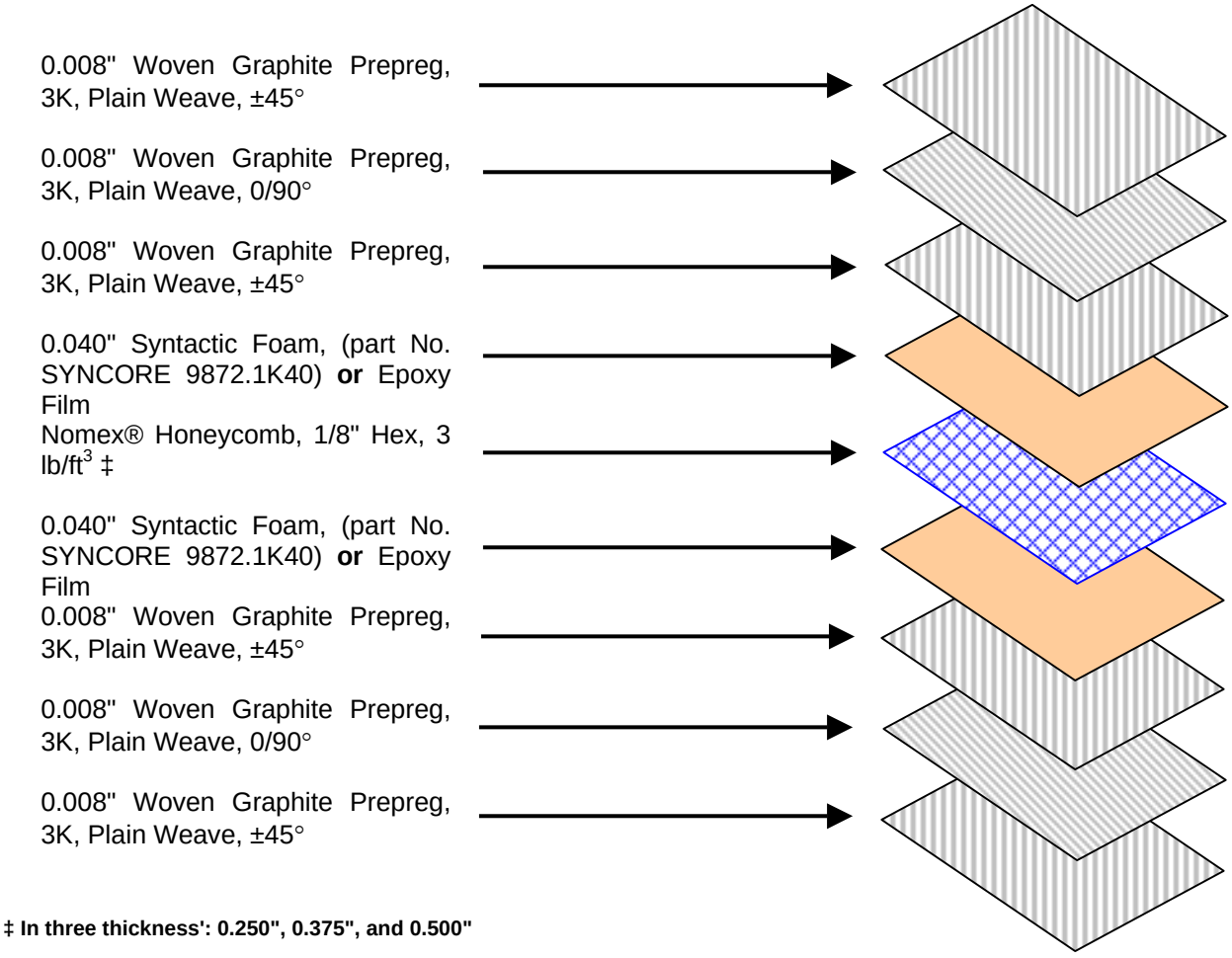
The ballistic testing of panels fabricated from aircraft materials will be performed by impacting fan blade fragments at velocities that are representative of an uncontained engine debris event. All fan blade fragments used in testing will be in the 1-3 lb range, and fabricated from actual engine fan blades supplied by an engine manufacturer. The nitrogen-powered gas gun, Missile Intercept Kinetic Energy Simulator (MIKES), will be used to project the fragments at velocities from 500-800 fps.

The ballistic response of four materials will be investigated. The projectile (fan blade) initial velocity, orientation at impact, and residual velocity of the fan blade fragment will be measured using high-speed film. For materials currently included in the UEDDAM code, the prediction accuracy of the code will be compared against the actual test data. For those materials that are not currently encompassed in the UEDDAM, the test data will be used to characterize the ballistic response and adapt the code to incorporate these new materials.

4.1. Test Article Description

The test articles are 3' x 3' size panels in four different materials: 1) honeycomb-cored composite, 2) 2024-T3 aluminum, 3) Ti-6AL-4V titanium, and 4) Inconel® 625 Low Cycle Fatigue (LCF) alloy. The composite panels are of a generic honeycomb-cored construction, designed with input from industry to be representative to current aircraft composite structures. APPENDIX B lists some composite lay-ups used in industry. Three different thickness' of honeycomb panels are to be tested: 1) 0.250", 2) 0.375", and 3) 0.500". The lay-up of the composite panels, noting the material type, thickness, and fiber direction are shown in Figure 1. A total of thirty (30) generic honeycomb-cored composite panels are to be fabricated for this test in the following quantities for each honeycomb thickness: twelve (12) in 0.250", twelve (12) in 0.375", and six (6) in 0.500". In addition to the generic composite panels, any panels supplied by industry will be tested. The generic composite panels are to be the baseline configuration to which the manufacturer-specific panels will be compared.

The quantity of metal panels required for this test is as follows: ten (10) each of 2024-T3 aluminum, ten (10) each of Ti-6AL-4V titanium, and five (5) of the Inconel® 625 LCF. A complete listing of the quantities and thickness of each type of metal is shown in Table 1.



‡ In three thickness': 0.250", 0.375", and 0.500"

Figure 1: Composite Panel Lay-up

Table 1: Metal Panel Materials List

Material	Thickness	Quantity
Aluminum 2024-T3	0.250"	5
	0.375"	5
Titanium Ti-6AL-4V	0.125"	5
	0.250"	5
Inconel® 625 LCF	0.063"	5

4.2. Test Matrix

Ballistic testing will be performed on four panel materials: 1) honeycomb-cored composite, 2) 2024-T3 aluminum, 3) Ti-6AL-4V titanium, and 4) Inconel® 625 LCF alloy. The separate test series are described below, with the complete test matrix shown in APPENDIX A. The test matrix outlines the proposed methods and procedures. However, the test engineer may make changes during the course of testing to optimize the use of assets, facilities, or personnel.

4.2.1. Systems Check-Out Tests

Two test shots will be performed prior to the commencement of the actual test series for checking that all systems are working correctly. These shots will be performed with blade fragments from previous testing. The high-speed film will be analyzed from the test shots, prior to the commencement of actual testing, to check for adequate lighting and flash bulb timing. In addition, the ability to impact the 36" square panel in the center at 20 ft will be investigated, and this distance reduced if deemed necessary. Surplus 0.0063" Ti-6AL-4V panels will be placed in the test stand to utilize these test shots as data points.

Table 2: Systems Check-out Test Series

Shot No.	Panel Type	Fragment Size (inches)	Fragment Velocity (fps)	Fragment Orientation (degrees)
1	Test	8 x 8	650	90
2	"	"	650	"

4.2.2. Composite Panel Tests

Composite panel testing is designed to obtain enough data to provide a database for incorporating composite materials within the UEDDAM code. To provide an effective database, the test matrix must encompass the many variables involved with ballistic impacts. Factors to consider for ballistic impacts are:

- Impacting Fragment's Physical properties:
  - Size
  - Shape
  - Mass
  - Material
- Ballistic Properties:
  - Velocity
  - Fragment impact orientation
  - Shotline obliquity
- Impacted Object's Properties
  - Material
  - Thickness

For the purposes of the UEDDAM code the impacting fragment is a turbine engine fan blade. Actual turbine engine fan blades are to be used in this test, thus solving the issue of material type and shape. Two fragment sizes are to tested: 1) 3" x 8", and 2) 8" x 8". These fragment sizes were selected as they are typical for an uncontained engine debris event.

The ballistic aspects of an uncontained engine debris event are defined as the velocity, orientation, and obliquity of the fragment. The velocity range considered necessary for testing is between 500 and 800 ft/s. Actual testing will be performed at these limits and at 650 ft/s. Fragment impact orientations are difficult to control for test purposes due to the instability of the fan blade, but it is desired to obtain 90° and 60° angles. Shotline obliquity angles shall be limited to 0° due to the limited number of panels available. Table 3 shows the desired test parameters for the composite panels used in the first test phase.

Table 3: Composite Panel Test Series

Shot No.	Panel Type	Fragment Size (inches)	Fragment Velocity (fps)	Fragment Orientation (degrees)
3	Generic Panel No. 1*	3 x 8	500	90
4	"	"	"	60
5	"	"	650	90
6	"	"	"	60
7	"	"	800	90
8	"	"	"	60
9	"	8 x 8	500	90
10	"	"	"	60
11	"	"	650	90
12	"	"	"	60
13	"	"	800	90
14	"	"	"	60
15	Generic Panel No. 2**	3 x 8	500	90
16	"	"	"	60
17	"	"	650	90
18	"	"	"	60
19	"	"	800	90
20	"	"	"	60
21	"	8 x 8	500	90
22	"	"	"	60
23	"	"	650	90
24	"	"	"	60
25	"	"	800	90
26	"	"	"	60
27	Generic Panel No. 3***	3 x 8	500	90
28	"	"	"	60
29	"	"	650	90
30	"	"	"	60
31	"	"	800	90
32	"	"	"	60

*** 0.250" Nomex® Honeycomb**
**** 0.375" Nomex® Honeycomb**
***** 0.500" Nomex® Honeycomb**

4.2.3. Aluminum Panel Tests

The second material type to be tested is 2024-T3 aluminum. Aluminum is a common metal used in aircraft construction and has recently been considered for use in component shielding. The UEDDAM code currently has the ability to determine the

ballistic response of aluminum 2024-T3. This testing shall serve to validate the existing penetration equations within the UEDDAM.

Due to the interest in using 2024-T3 aluminum for component shielding, the emphasis of this testing is to validate the V_{50} velocity value rather than to obtain residual velocities. V50 is defined as the velocity at which the fragment has 50% a chance of penetrating the shielding. Verification of the UEDDAM's V_{50} for aluminum will provide industry with a validated design tool for component shield sizing (thickness) requirements.

Only larger fragments (8" x 8") will be tested as these present the greatest challenge for component shielding. Fragment velocities will be tested around the V_{50} for the 0.250" and 0.375" thick 2024-T3 aluminum. Figure 2 and Figure 3 shows UEDDAM predicted values for V_{50} with respect to fragment orientation and obliquity for the 0.250" and 0.375" thick aluminum panels, respectively. The test matrix for this series is shown in Table 4.

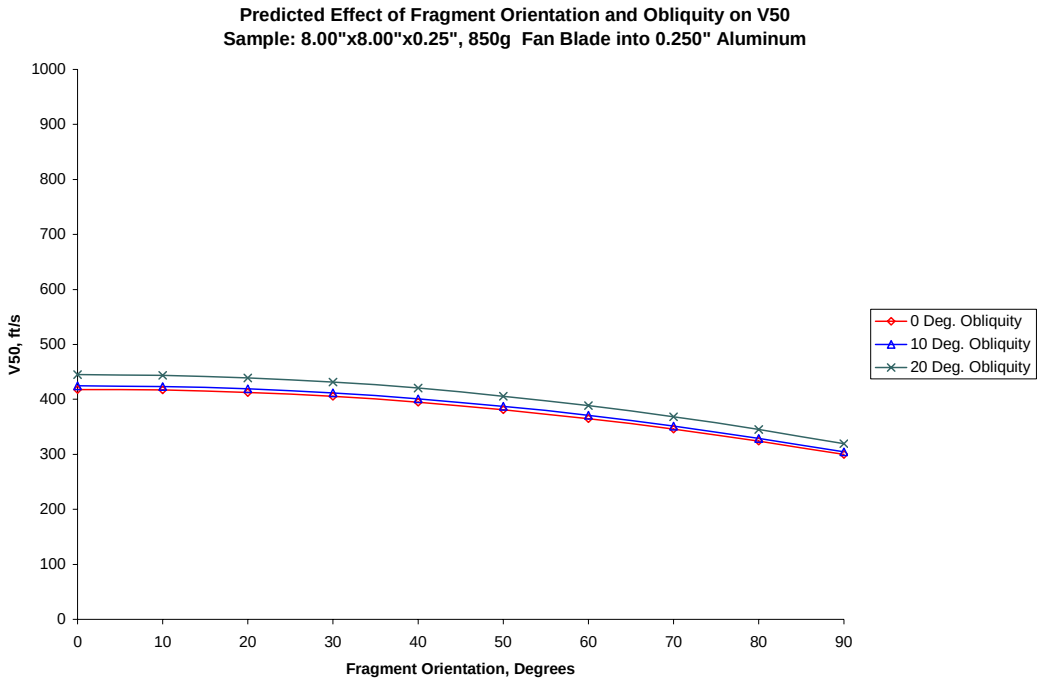


Figure 2: Predicted V_{50} for 0.250" Aluminum

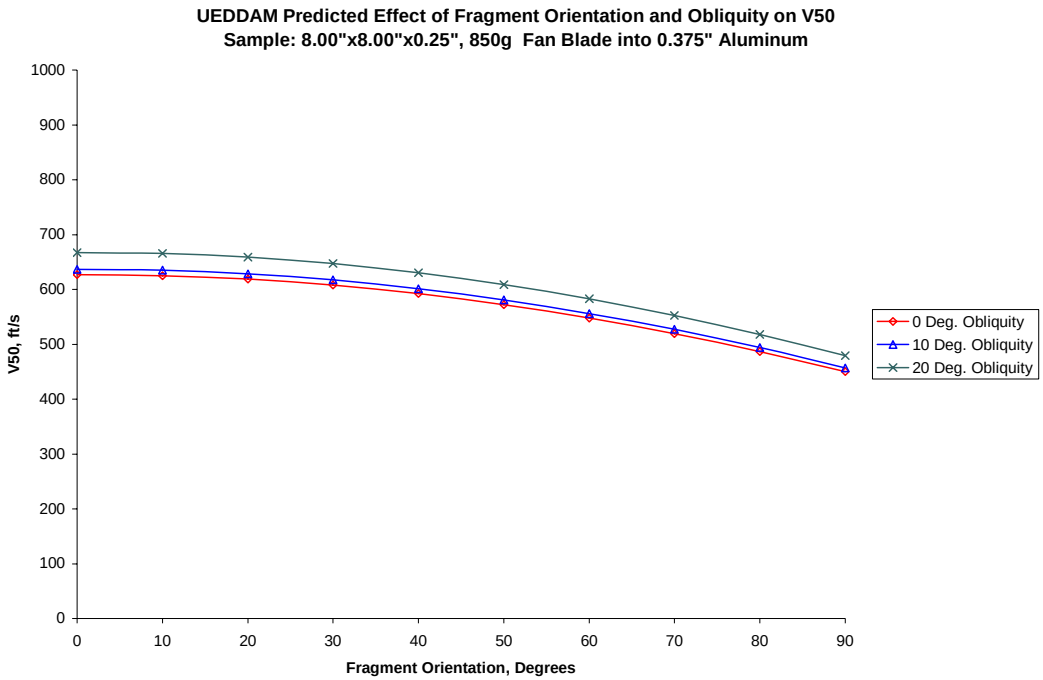


Figure 3: Predicted V_{50} for 0.375" Aluminum

Table 4: Aluminum 2024-T3 Panel Test Series

Shot No.	Panel Type	Fragment Size (inches)	Fragment Velocity (fps)	Fragment Orientation (degrees)
33	0.250" Aluminum	8 x 8	300	90
34	"	"	300	"
35	"	"	305	"
36	"	"	310	"
37	"	"	TBD	"
38	0.375" Aluminum	"	450	"
39	"	"	450	"
40	"	"	455	"
41	"	"	460	"
42	"	"	TBD	"

4.2.4. Titanium Panels Tests

Ti-6AL-4V titanium will be evaluated in the third test series to validate the existing prediction capability of the UEDDAM code for this material. Titanium is also being considered for use in fuel tank armoring and component shielding. To validate the penetration equations in a manner that supports industry, the test will consider only larger fragments (8" x 8") in the V_{50} region for the material. Larger fragments are representative of the fan blades being incorporated in the newer high efficiency turbines used in long range aircraft, where increased fuel capacity is necessary. The predicted V_{50} for 0.125" titanium impacted with an 8" x 8" fragment, at a 90° fragment angle and

0° obliquity is 327 ft/s (as shown in Figure 4). The first two shots (No.'s 43 and 44) are to be performed at the approximate V_{50} point. Successive shots will be performed at higher velocities in 5 ft/s increments. The 0.250" titanium will be tested in the same manner, with the first two shots (No.'s 48 and 49) at approximately the V_{50} value of 654 ft/s (see Figure 5). Additional shots will be performed at incremental velocities. The test matrix for this series of testing is listed in Table 5.

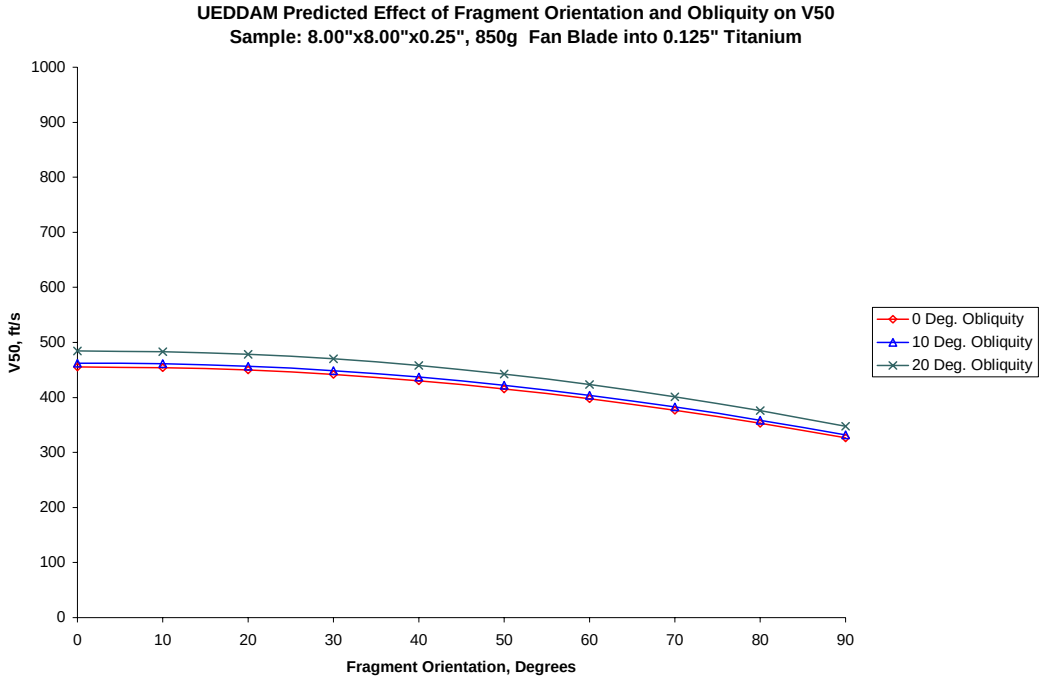


Figure 4: Predicted V_{50} for 0.125" Titanium

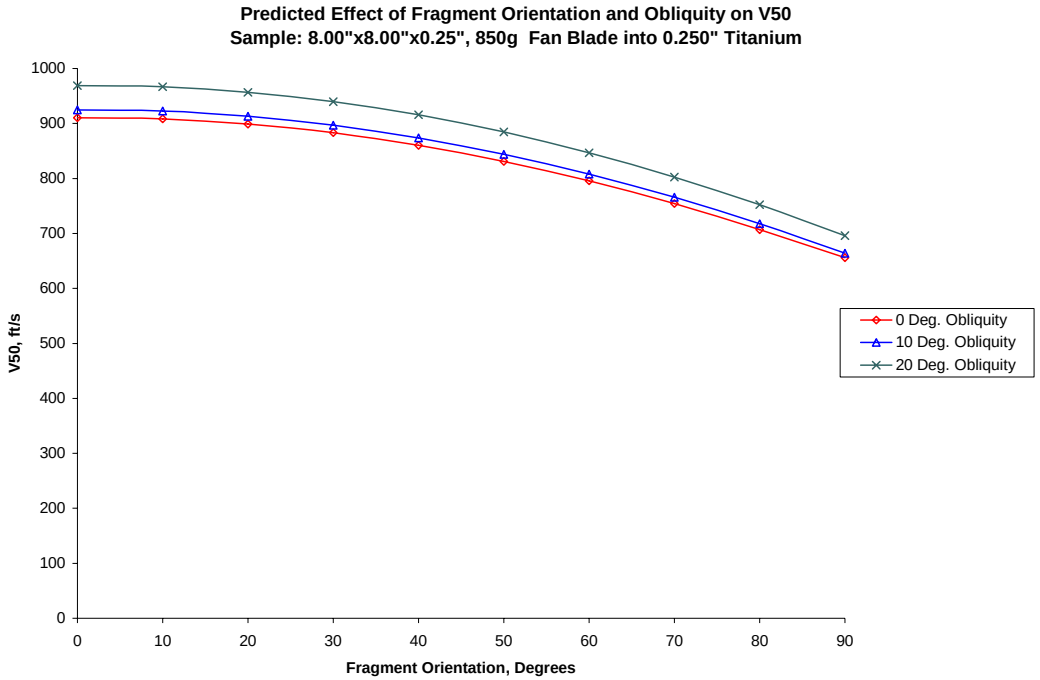


Figure 5: Predicted V_{50} for 0.250" Titanium

Table 5: Titanium Ti-6AL-4V Panel Test Series

Shot No.	Panel Type	Fragment Size (inches)	Fragment Velocity (fps)	Fragment Orientation (degrees)
43	0.125" Titanium Ti-6AL-4V	8 x 8	330	90
44	"	"	330	"
45	"	"	335	"
46	"	"	340	"
47	"	"	TBD	"
48	0.250" Titanium Ti-6AL-4V	"	650	"
49	"	"	650	"
50	"	"	655	"
51	"	"	660	"
52	"	"	TBD	"

4.2.5. Inconel Panel Tests

The Inconel® 625 LCF panels are to be evaluated in a similar fashion as the composite for inclusion in the UEDDAM code. These materials have also been considered for use in shielding critical components. Testing will attempt to obtain some initial characterization of the ballistic response of this material. The test matrix for this series is shown in Table 6.

Table 6: Inconel® 625 LCF Panel Test Series

Shot No.	Panel Type	Fragment Size (inches)	Fragment Velocity (fps)	Fragment Orientation (degrees)
53	0.063" Inconel® 625 LCF	8 x 8	500	90
54	"	"	"	60
55	"	"	650	90
56	"	"	"	60
57	"	"	800	90

4.3. PRE-TEST PREDICTIONS

No in depth pre-test predictions are to be calculated for this test. The composite panels and the Inconel® 625 LCF are currently not contained within the UEDDAM code, making it impossible to perform predictions for these materials. For those materials contained within the UEDDAM (titanium and aluminum), some rough pre-test predictions were performed to determine the V_{50} for each material. These predictions are shown in the previous section and were utilized to determine the velocities at which the materials would be tested.

Accurate and meaningful pre-test predictions, using the penetration equations from the UEDDAM code, would require knowing the impact orientation and velocity of the fragment to some degree of accuracy. Whilst both the fragment orientation and initial velocity are specified in the test matrix, it is very difficult to accurately meet these criterion in actual testing. Thus, Figure 2 and Figure 5 are provided to predict the expected residual velocity ranges only. Actual comparison of residual velocity predictions to actual test residual velocities will be conducted in the post-test analysis. Post-test analysis of the high-speed film will provide the most accurate fragment orientation and impact velocity data for input into the penetration equations.

4.4. PRE-TEST PREPARATION AND SETUP

4.4.1. Test Specimen Preparation

The test panels will require holes drilled in them so that they can be bolted to the test stand. Any manufacturer-specific panels will be custom-fitted as they become available.

The fan blade fragments will be cut form several complete blade assemblies. The approximate dimensions of these fan blades are shown in Figure 6. Several of these blades are available for testing. However, only two blades will be cut prior to the test. Figure 7 illustrates the desired cutting pattern, providing two (2) blades of approximately 3" x 8" dimension (Sections 1 and 3) and one (1) blade of approximately 8" x 8" (Section 2). Vibration dampening fins will be removed. The root section of the blade (section 4) will be saved for possible use in follow-on testing.

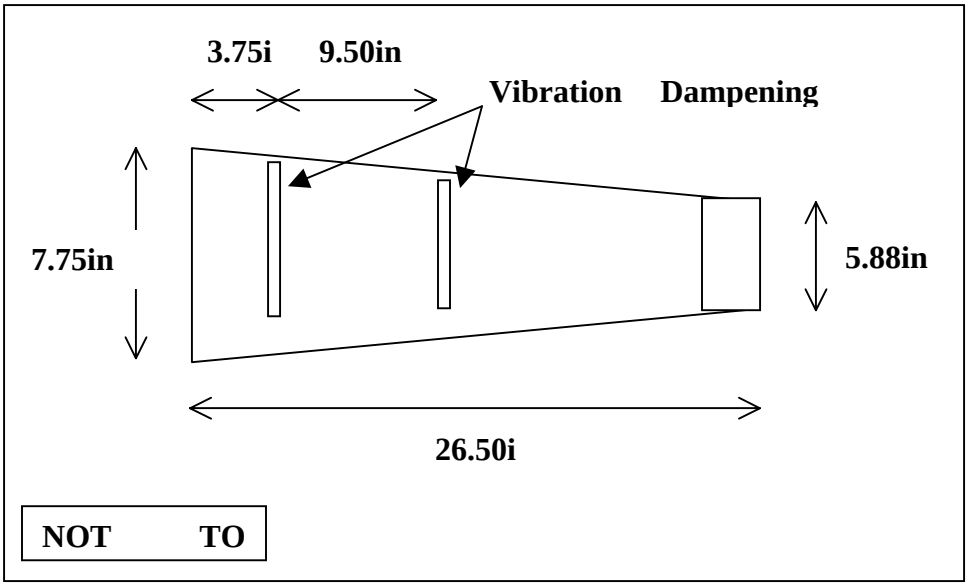


Figure 6: Complete Fan Blade Dimensions

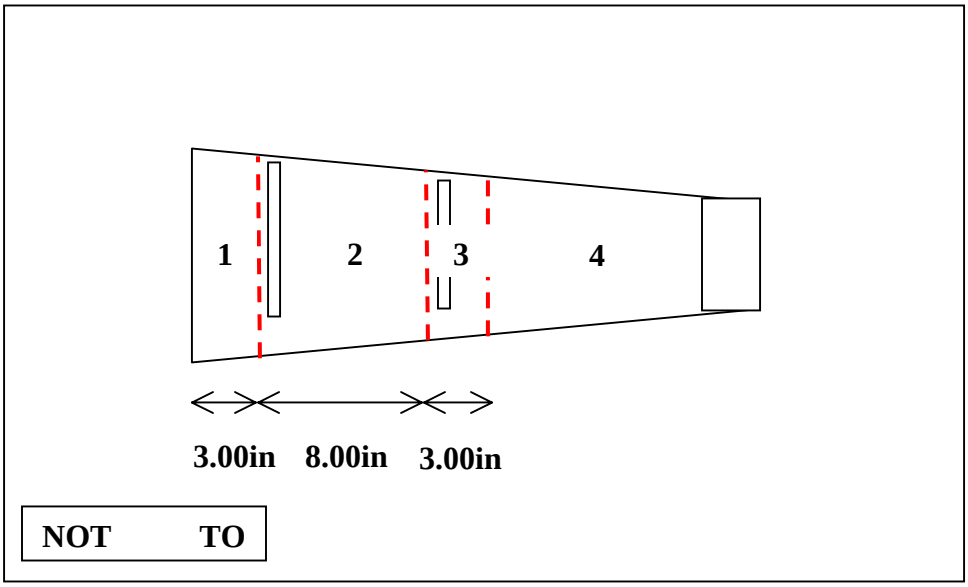


Figure 7: Suggested Cutting Pattern for Fan Blades

4.4.2. Test Facility Requirements

The Weapons Survivability Laboratory (WSL) at the Naval Air Warfare Center Weapons Division (NAWCWD) in China Lake, CA will be the test facility. The K-2 site will be utilized for this test. This facility is more cost-effective than using the main site and is adequately instrumented and powered for this test.

4.4.3. Test Pad Setup

The equipment required to perform this test is as follows: 1) the MIKES gun, 2) sabot catcher/stripper, 3) test stand, and 4) celotex® bundles. Figure 8 shows the proposed test pad setup.

The MIKES gun is a nitrogen-powered gas gun at the WSL test facility. The 12" bore barrel extension will have to be added to the MIKES gun to enable testing the 8" x 8" fragments. This extension shall be in place throughout testing, even when using the smaller 3" x 8" fragments, thus requiring the fabrication of only one standard sabot.

A combination of a sabot catcher and a sabot stripper will be utilized for this test. The sabot stripper will be attached to the muzzle of the MIKES gun barrel extension, at approximately 1 ft from the end of the barrel. The function of the sabot stripper is to stop the teflon® base plate of the sabot and the steel sabot ring from continuing down range. Very little of the foam filling will be stopped by the sabot stripper.

The secondary sabot catcher will be placed approximately 5 ft from the muzzle. This catcher has a cutout that is slightly larger than the cutout of the sabot stripper sabot stripper. The enlarged cutout allows for some possible deviation of the fragment from the shotline. The role of this second sabot catcher is to stop as much of the foam from impacting the test panels. An additional function of this sabot catcher is to reduce the effects of the shock wave from the MIKES gun on the test panel.

The test stand must be capable of firmly attaching the test panels and rigid enough that it does not move due to the blast from the MIKES gun. It is desired to have the test stand tall enough to be able to mount the test panels with their center level with the shotline. Every attempt should be made to utilize or modify an existing test fixture, rather than fabricating one from scratch. One constraint in the design of the test stand is that it must allow for an unobstructed FOV for the high-speed cameras on both the entrance (impact) and exit (residual) sides of the test panel.

A bundle of celotex® will be placed in the shotline behind the test panel to capture the fan blade fragment for re-use. This material comes in a palletized form and can be replaced during the test as it deteriorates through use.

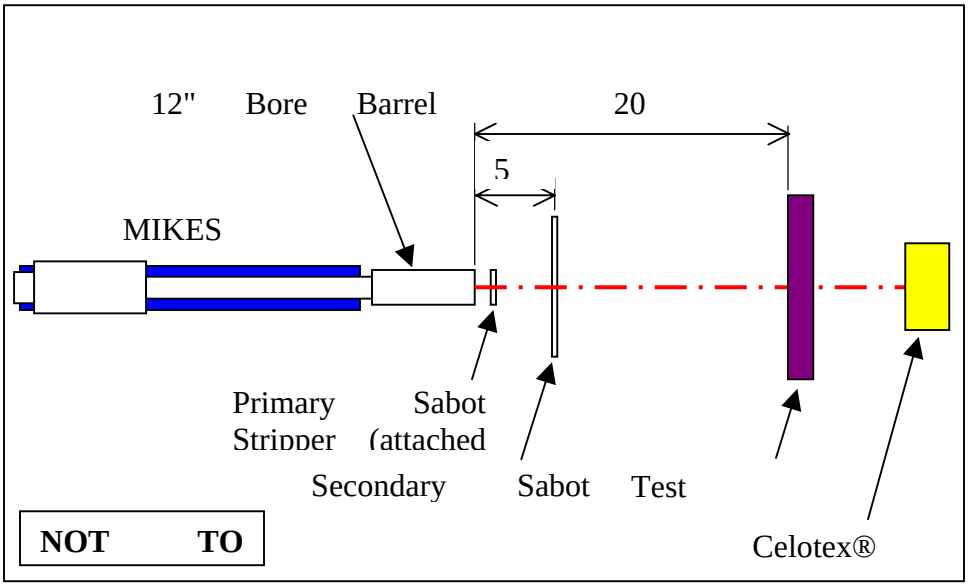


Figure 8: Test Pad Setup

4.5. DATA REQUIREMENTS

The primary data to be acquired from this testing are as follows: the fragment 1) impact velocity, 2) residual velocity, and 3) orientation at impact. This data will be obtained from high-speed film of both the entrance (impact) and exit (residual) sides of the test panel.

Some additional data may be obtained during the test on the performance of the firing system for the MIKES gun. For each shot the delay time of the firing system from initiation to the projectile exiting the barrel will be acquired and noted for historical record. This delay time is used in setting up the timing of the flash bulbs and high-speed photography. The current estimate for the firing system delay is 75 ms, but this has never been verified. In addition to the delay time of the firing system, the performance of the break-wire at the muzzle will also be evaluated using high-speed film. This additional data will require a third high-speed camera. Due to the cost of an additional camera and film processing, this data will only be recorded for one or two shots.

4.5.1. Instrumentation

Test facility instrumentation will include standard range facility instrumentation, with the addition of high-speed cameras. One range channel will be utilized for the firing line, to initiate the MIKES gun. Instrumentation requirements are itemized as follows:

- Air gun delta pressure velocity
- High speed camera No. 1

- High speed camera No. 2
- High-speed camera No. 3 (for breakwire analysis on some shots)
- 6,000 Watts of light (6 PAR64 lamps)
- Range safety video
- Air gun controlling and monitor
- Flash bulbs (4 PF-300 Meggaflash lamps)
- Electronic strobe (fire pulse triggered)

4.5.1.1. High Speed Film

The high-speed photography is a crucial piece of test instrumentation for this test, being used to obtain the following projectile data: 1) impact velocity, 2) impact orientation, and 3) residual velocity. The failure to obtain one aspect of the projectile data will void the shot as a data point. Thus, achieving the greatest quality high-speed film images is important for test fidelity.

Setup of the high-speed film for testing, is based on three factors: 1) setting up the camera, 2) placement of the camera, and 3) the lighting requirements. All three factors are not independent of one another, however, for clarity they will be discussed separately.

The setup of the camera is primarily driven by the velocity of the object to be filmed. Object velocity determines what combination of shutter index and film speed is required to obtain an acceptable blur length. Minimizing the blur length improves the fidelity of the post-test velocity and fragment angle measurement. The relationship of object velocity, shutter index, film speed, and blur length are shown by the equations,

$$Speed_{Shutter} = Index_{Shutter} \bullet Speed_{Film}$$

$$Length_{Blur} = \frac{V_{Object}}{Speed_{Shutter}}$$

The number of pictures per foot in the field of view (FOV) is also an important factor in determining what shutter speed is required. This aspect is calculated by the following,

$$\#Pictures_{ft.FOV} = \frac{Speed_{Film}}{V_{Object}}$$

Experience from previous testing in the FAA Catastrophic Failure Prevention Program has shown that it is desired to run the high-speed cameras at a film speed no faster than 6000 pps (pictures per second). Although these high-speed cameras can run at film speeds close to 10000 pps, they are more prone to failures and increased wear when run at their maximum speeds. A film speed of 6000 pps combined with a shutter index of 2.5, achieve a blur length of 0.40" and 0.64" at object velocities of 500 ft/s and 800 ft/s, respectively. These blur lengths have been deemed acceptable for larger

fragments (approx. 8"). Table 7 shows the initial high-speed camera setup parameters for this test.

Table 7: High-Speed Film Setup Parameters

Object Velocity (ft/s)	Shutter Index (No.)	Film Speed (pps)	Shutter Speed (s^{-1})	Shutter Duration (ms)	Blur Length (in)	Pictures per ft FOV (pic/ft)
500	2.5	6000	15000	66.7	0.40	12.00
650	2.5	6000	15000	66.7	0.52	9.23
800	2.5	6000	15000	66.7	0.64	7.50

The next step is to determine the camera placement and lens required for the high-speed cameras. The placement of the camera must be such that a sufficiently large enough viewing width exists from which to obtain the velocity measurements. In determining the necessary viewing width, consideration must also be given to the number of pictures per foot FOV, calculated previously. The FOV angle is a function of the focal length of the lens used and the width of the film image, and is expressed as,

$$FOV = 2 \bullet \arctan\left(\frac{Width_{Film_Image}}{2 \bullet Length_{Lens-Focal}}\right)$$

The placement distance of the camera from the object can be determined from the necessary FOV width criteria. Where, FOV width can be calculated using the following trigonometry (see Figure 9),

$$Width_{FOV} = 2 \bullet Length_{View_Distance} \bullet \tan\left(\frac{FOV}{2}\right)$$

Previous testing showed that placing the cameras 10 ft from the shotline was necessary to reduce the effects of the shock-wave from the gun and to minimize the prospect that the cameras would be damaged by debris. In addition, placing the cameras any further away than 10 ft would reduce the clarity of the picture for post-test analysis. The WSL currently has available lens' for the high-speed cameras with focal lengths of: 24mm, 45mm, and 100mm. Standard image width for the film used is 0.43". The FOV width at 10 ft, using the standard film image width, is shown in Table 8 with respect to the different lens focal lengths. High-speed film will be 16mm Kodak High Speed Ektachrome, EI 400, 250 ft roll, Spec 432.

The high-speed camera setup for this test is shown in Figure 10. Projectile velocity measurement requires the film to provide at least two clear frames, preferably with the projectile of equal distance from the center of the FOV to reduce errors due to parallax. For simplicity in the post-test analysis, it is desired have the FOV centerline perpendicular to the shotline. The camera FOV centerline shall be placed 1.5 ft from the impact plane, so that the test panel is within the FOV of the camera. During the

camera setup the FOV width at 10 ft should be noted and used as a comparison or validation of the equations used for setup.

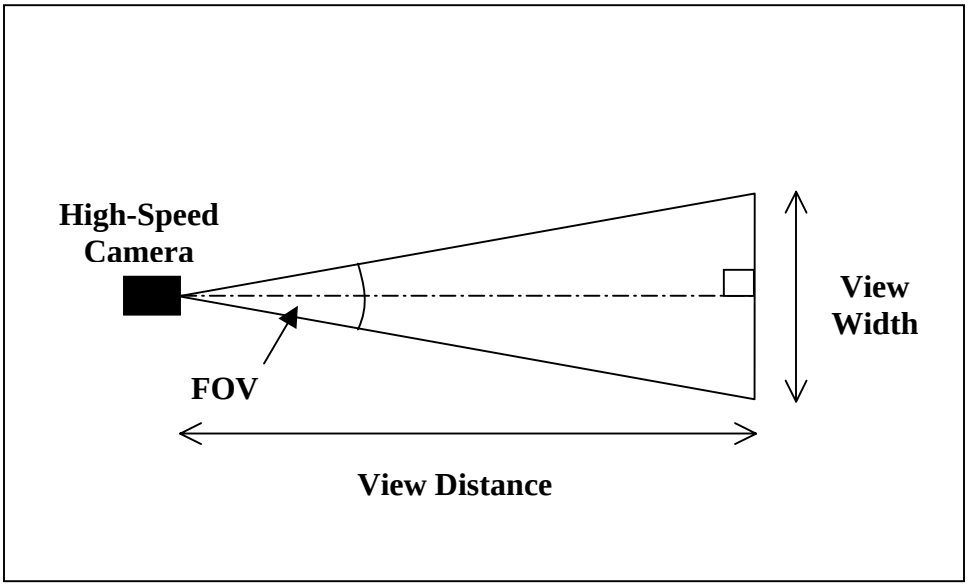


Figure 9: Camera Setup Geometry

Table 8: FOV Width and Pictures per FOV Width

Image Width (in)	Lens Focal Length (mm)	Field of View Angle (°)	View Distance (ft)	FOV Width at View Distance (ft)	Pictures per FOV Width (pics)
0.43	24	24.8	10	4.39	32.9
0.43	45	13.3	10	2.34	17.6
0.43	100	6.0	10	1.05	7.9

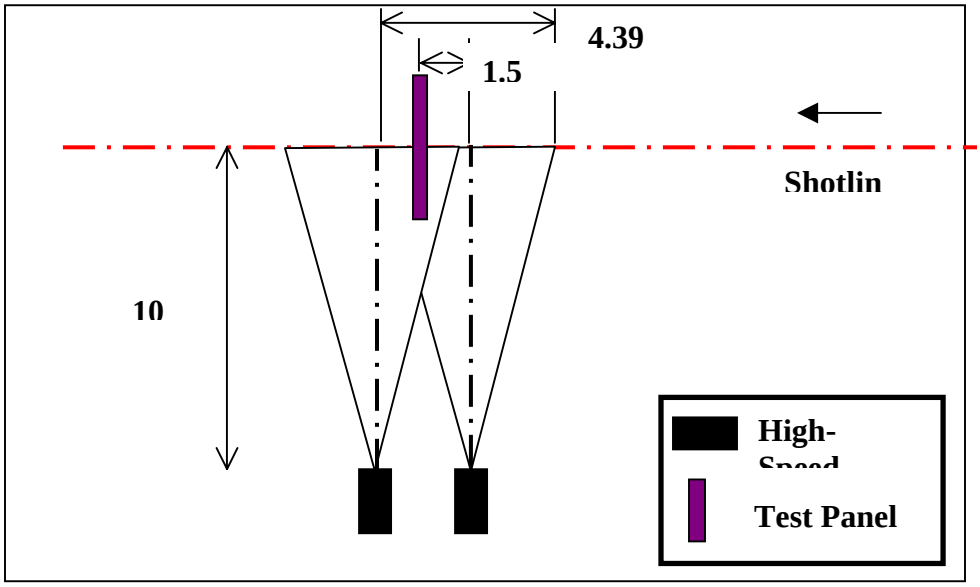


Figure 10: Camera Setup Dimensions (24mm Focal Length Lens)

The high-speed cameras will be timed with respect to the MIKES gun fire signal (t=0). With the cameras setup to run at 6000 pps, the cameras need to be up to their designated speed by the time the fragment has entered the FOV. Table 9 shows the timeline for the initiation of the high-speed cameras with respect to fire signal for the three standard fragment velocities to be used in the composite test series. The initiation time for other velocities will be determined by the project engineer prior to the shot.

Table 9: Time Line for HS Cameras with Respect to Fire Signal

Fragment Velocity (ft/s)	HS Camera Delay (@6000 pps) $t_{HS\ Camera}$ (ms)	Fire Signal (t=0) $t_{Fire\ Signal}$ (ms)	Breakwire $t_{Breakwire}$ (ms)	Flash Bulb Initiation $t_{Flash\ Bulb}$ (ms)	Fragment Impact t_{Impact} (ms)
500	-1385.0	0.0	75.0*	93.0	115.0
650	-1394.2	0.0	75.0*	83.8	105.8
800	-1400.0	0.0	75.0*	78.0	100.0

***Approximate value from previous testing**

Two (2) flash bulbs are required to provide adequate lighting per camera, so that four (4) flash bulbs in total will be needed per shot. The timing of these flash bulbs is critical as the light output spans only 30 ms. Initiation of these flash bulbs will require the use of the flash timer equipment to obtain millisecond accuracy. Table 10 shows the timeline for the initiation of the flash bulbs with respect to the breakwire. The initiation time for other velocities will be determined by the project engineer prior to the shot. The data for the high-speed cameras and flash bulbs was determined from previous FAA testing and is referenced in APPENDIX C.

Table 10: Time Line for Flash Bulbs with Respect to Breakwire

Fragment Velocity (ft/s)	HS Camera Delay (@6000 pps) $t_{HS\ Camera}$ (ms)	Fire Signal (t=0) $t_{Fire\ Signal}$ (ms)	Breakwire $t_{Breakwire}$ (ms)	Flash Bulb Initiation $t_{Flash\ Bulb}$ (ms)	Fragment Impact t_{Impact} (ms)
500	-1460.0	-75.0*	0.0	18.0	40.0
650	-1469.2	-75.0*	0.0	8.8	30.8
800	-1475.0	-75.0*	0.0	3.0	25.0

***Approximate value from previous testing**

In addition to the flash bulbs, six PAR64 lamps will also be used (3 per camera). The purpose of the PAR64 lamps is twofold: 1) to provide an alternative light source, and 2) for increasing the general distribution of light in the FOV. The PAR64 lamps should provide enough light to be able to obtain velocity measurements from the film during the post-test film analysis in the event of a flash bulb failure. The additional lighting provided by the PAR64 lamps should also disperse light throughout the FOV, thus reducing the dark spots in the background areas, and produce better quality film products.

A background board with a grid pattern will be utilized for this test, but with several modifications due to experience from previous testing under the FAA Catastrophic Failure Mitigation Program. The reflective paint used on background boards in previous tests produced considerable glare on the high-speed film. This glare sometimes partially obscured the fragment during the post-test film analysis. For this test the background board shall be painted a flat white, to utilize the reflective properties of white and to minimize the glare due to the surface finish. The grid pattern shall be in 1 ft sized squares with the black lines being no thicker than 0.500". In addition to the background board, two flat white painted boards (one in front of the test panel and one behind) shall be placed on the test pad below the shotline to reflect light on the underside of the fragment, as shown in Figure 11. These boards will have to be restrained to avoid moving due to the blast of the MIKES gun.

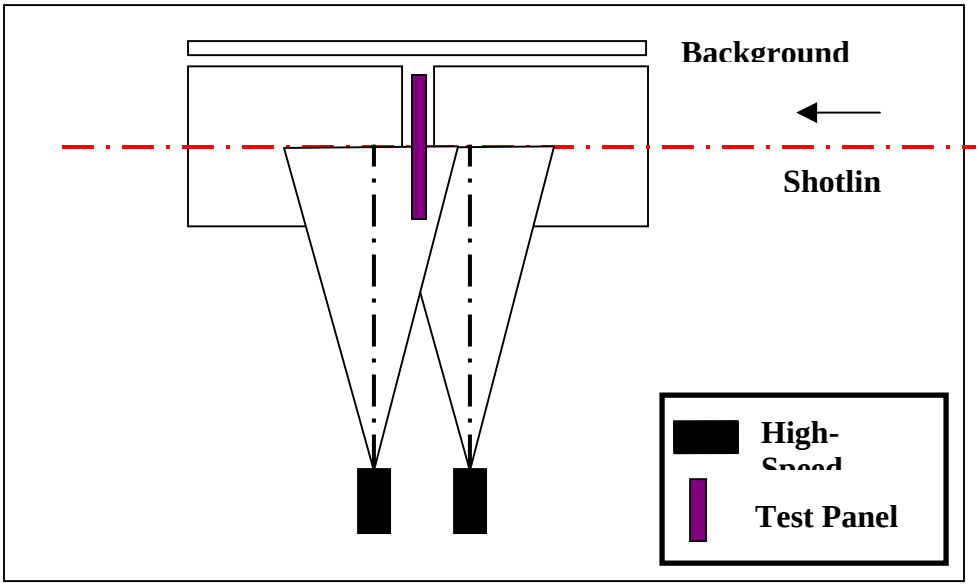


Figure 11: Background Board Setup

A lighting setup consisting of four (4) flash bulbs and six (6) PAR64 lamps will be used for each shot. This desired lighting setup is shown in Figure 12. The flash bulbs shall be placed one on either side of the high-speed cameras, with their beams focused to the same point (approximately 1 ft from the FOV centerline). The PAR64 lamps are to be placed alongside the high-speed cameras, but not in between them due to space constraints. These lamps shall be aimed at different locations on the background board to provide the greatest coverage of light. If time permits, a special fixture shall be constructed to hold the PAR64 lamps firmly so that they should not need to be adjusted after every shot.

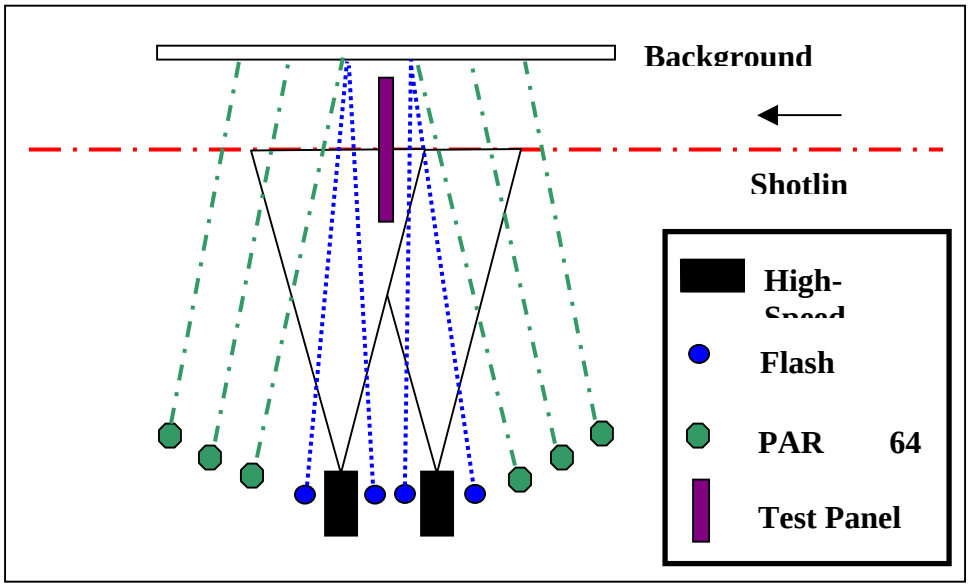


Figure 12: Test Pad Lighting Setup

An electronic strobe light will be placed within the camera FOV on the impact side of the test panel. The strobe will be connected to flash once with signal of the MIKES gun fire pulse. This flash will aid in the high-speed film analysis.

4.5.2. Optical and Audio Records

A combination of standard and digital photography will be utilized in this test for both pre- and post-shot documentation. Digital photography reduces the time and cost of inserting pictures within presentations and reports. For historical reference, pre-shot pictures will be taken of the following:

1. Blade Fragment
2. Sabot
3. Test panel
4. Test pad setup

Post-test pictures will be taken of the following:

1. Entrance side of test panel
2. Exit side of test panel
3. Blade fragment (if found)

All pictures will include a 3" x 5" note card (or similar), referencing the shot number, and a length of tape measure or a scale.

4.6. TEST PROCEDURE

The following is a sequential outline of the test procedures:

- Document setup
- Sight MIKES gun
- Take pre-test photographs
- Prepare MIKES gun for firing
- Sight high-speed cameras and PAR64 lamps and flash bulbs
- Evacuate test pad of all nonessential personnel
- Charge MIKES gun with desired nitrogen firing pressure
- Commence data recording
- Fire MIKES gun
- Stop data recording
- Document impact damage to test panel
- Take post-test photographs
- Salvage fan blade fragment from celotex® bundles

5. TEST CONSTRAINTS

5.1. ENVIRONMENTAL

All testing will be accomplished when adequate light is available for the video camera. The test will be stopped in the event of the following:

- Winds in excess of 25 knots
- Rain or overcast conditions

5.2. SAFETY AND SECURITY

Safety equipment must be operational during the test. This includes video cameras used for safety video. All personnel are to wear coveralls when on the test pad.

Tests will be conducted following standard operating procedures prepared by the WSL and approved by the NAWC Safety Office. Safety equipment for this test will include, but not be limited to: flame retardant coveralls, safety glasses, and standard ordnance grounding. At no time during the tests will project requirements overrule the safety of personnel or present hazards to the test facility. Any situation that the firing officer or project engineer feels threatens the safety of personnel, facility, or test items will be cause for a delay in testing. The Weapons Survivability Laboratory (WSL), Naval Air Warfare Center (NAWCWPNS), will consolidate the technical requirements of the test plan into a NAWCWPNS-approved operating procedure. This procedure will be used for all test runs in the test program.

5.3. LOGISTICAL

Failure of critical test or safety equipment will stop the test until repair is done.

6. DOCUMENTATION

This test will be documented with a photographic reference, high-speed film, digital video, and a final test report. The photographic reference will be a combination of still and digital photography. The final report will include a description of the test and results as well as a post-test analysis.

APPENDIX A
TEST MATRIX

Table A1-1a: Complete Test Matrix

Shot No.	Panel Type	Fragment Size (inches)	Fragment Velocity (fps)	Fragment Orientation (degrees)
1	Test	8 x 8	650	90
2	"	"	650	"
3	Generic Panel No. 1*	3 x 8	500	"
4	"	"	"	60
5	"	"	650	90
6	"	"	"	60
7	"	"	800	90
8	"	"	"	60
9	"	8 x 8	500	90
10	"	"	"	60
11	"	"	650	90
12	"	"	"	60
13	"	"	800	90
14	"	"	"	60
15	Generic Panel No. 2**	3 x 8	500	90
16	"	"	"	60
17	"	"	650	90
18	"	"	"	60
19	"	"	800	90
20	"	"	"	60
21	"	8 x 8	500	90
22	"	"	"	60
23	"	"	650	90
24	"	"	"	60
25	"	"	800	90
26	"	"	"	60
27	Generic Panel No. 3***	3 x 8	500	90
28	"	"	"	60
29	"	"	650	90
30	"	"	"	60
31	"	"	800	90
32	"	"	"	60
33	0.250" Aluminum	8 x 8	300	90
34	"	"	300	"
35	"	"	305	"
36	"	"	310	"
37	"	"	TBD	"
38	0.375" Aluminum	"	450	"
39	"	"	450	"
40	"	"	455	"
41	"	"	460	"
42	"	"	TBD	"
43	0.125" Titanium Ti-6AL-4V	8 x 8	330	"
44	"	"	330	"
45	"	"	335	"
46	"	"	340	"
47	"	"	TBD	"
48	0.250" Titanium Ti-6AL-4V	"	650	"
49	"	"	650	"
50	"	"	655	"
51	"	"	660	"
52	"	"	TBD	"

Table A1-1b: Complete Test Matrix (continued)

Shot No.	Panel Type	Fragment Size (inches)	Fragment Velocity (fps)	Fragment Orientation (degrees)
53	0.063" Inconel® 625 LCF	8 x 8	500	90
54	"	"	"	60
55	"	"	650	90
56	"	"	"	60
57	"	"	800	90

*** 0.250" Nomex® Honeycomb**
**** 0.375" Nomex® Honeycomb**
***** 0.500" Nomex® Honeycomb**

APPENDIX B
MANUFACTURER-SPECIFIC COMPOSITE LAYUPS

Manufacturer-Specific Composite Panel A & B

Lay-up:

Honeycomb Areas (Most of nacelle area),	Non Honeycomb Area (Around edges of doors and fixed panels, localized other areas.)
Outside Surface	**Outside Surface**
.008 Woven Graphite Prepreg with conductive aluminum fibers, .008" thick, ±45°	.008 Woven Graphite Prepreg with conductive aluminum fibers, .008" thick, ±45°
.008 Woven Graphite Prepreg, .008" thick, 0/90°	.008 Woven Graphite Prepreg, .008" thick, 0/90°
.008 Woven Graphite Prepreg, .008" thick, ±45°	008 Woven Graphite Prepreg, .008" thick, ±45°
.040 Epoxy Syntactic Foam	Film Adhesive
.500" Nomex Honeycomb, 1/8" Hex, 3 lb/cu ft	008 Woven Graphite Prepreg, .008" thick, 0/90°
.040 Epoxy Syntactic Foam	
008 Woven Graphite Prepreg, .008" thick, 0/90°	.008 Woven Graphite Prepreg, .008" thick, ±45°
.008 Woven Graphite Prepreg, .008" thick, ±45°	.005 Type 120 Fiberglass Prepreg
Bondable tedlar moisture barrier	Bondable tedlar moisture barrier
Inside Surface	**Inside Surface**

Manufacturer-Specific Composite Panel C & D

Lay-up:

Honeycomb Areas (Approximately 50% of nacelle area),	Non Honeycomb Area (Around edges of doors and fixed panels, and other areas approximating 50% total).
Outside Surface	**Outside Surface**
.008 Woven Graphite Prepreg with conductive aluminum fibers, .008" thick, ±45°	.008 Woven Graphite Prepreg with conductive aluminum fibers, .008" thick, ±45°
.008 Woven Graphite Prepreg, .008" thick, 0/90°	.008 Woven Graphite Prepreg, .008" thick, 0/90°
.040 Epoxy Syntactic Foam	Film Adhesive
.375" Nomex Honeycomb, 1/8" Hex, 4 lb/cu ft	008 Woven Graphite Prepreg, .008" thick, 0/90°
.040 Epoxy Syntactic Foam	
008 Woven Graphite Prepreg, .008" thick, 0/90°	.008 Woven Graphite Prepreg, .008" thick, ±45°
.008 Woven Graphite Prepreg, .008" thick, ±45°	.005 Type 120 Fiberglass Prepreg
Bondable tedlar moisture barrier	Bondable tedlar moisture barrier
Inside Surface	**Inside Surface**

APPENDIX C
TIME PLOTS FOR HIGH-SPEED CAMERAS AND FLASH BULBS

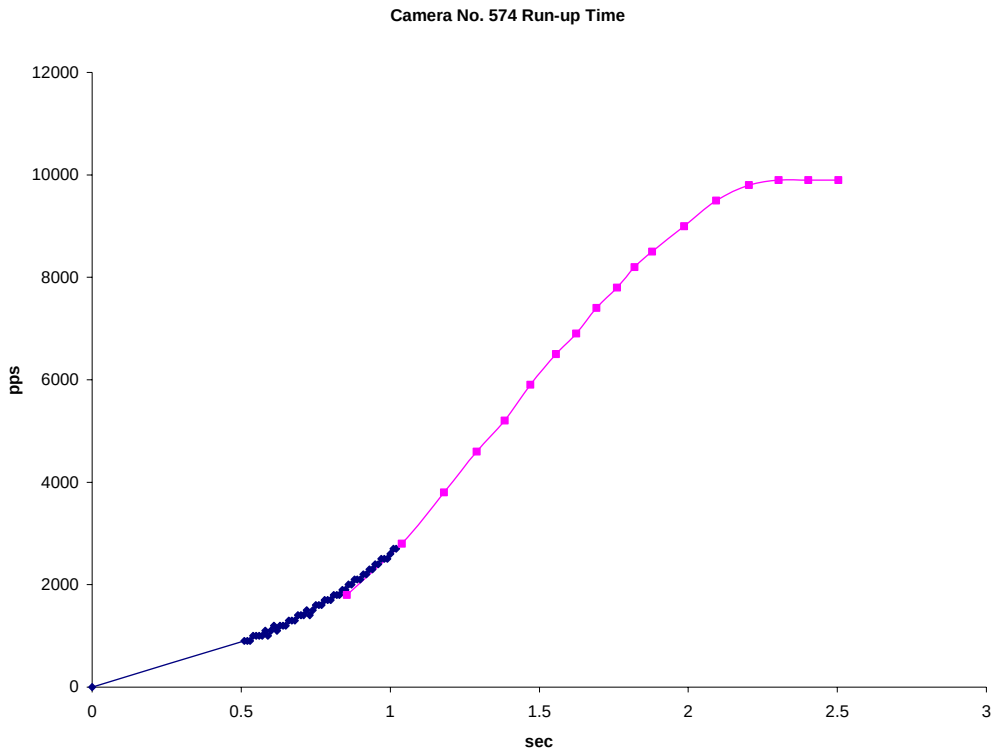


Figure C1: High-Speed Camera Run-up (Camera No. 574)

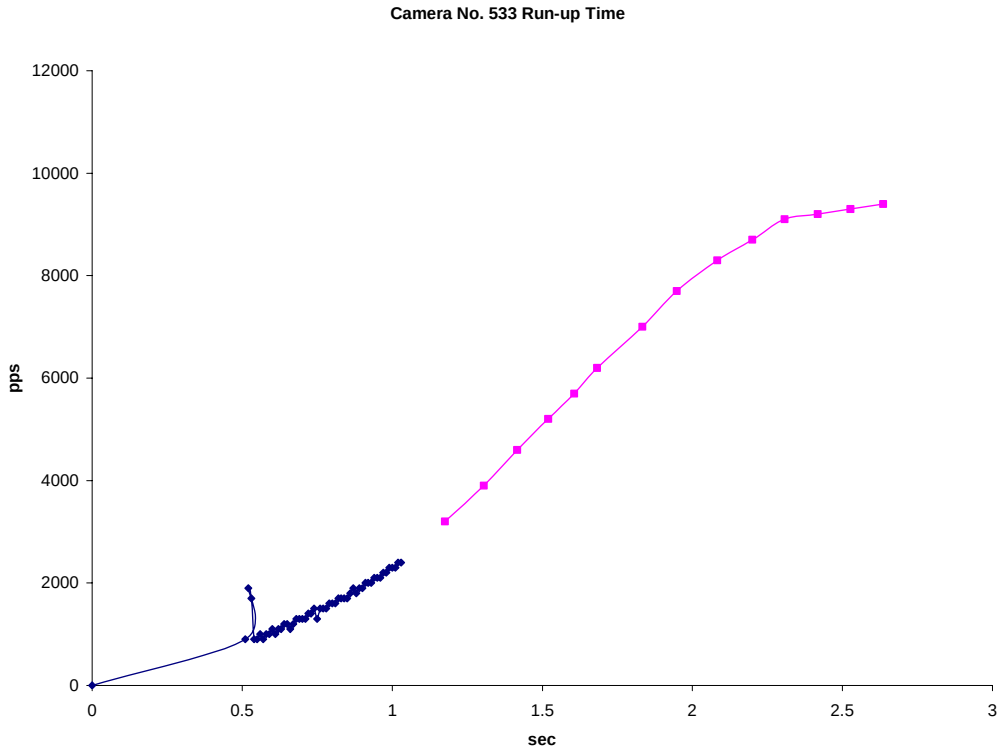


Figure C2: High-Speed Camera Run-up (Camera No. 533)

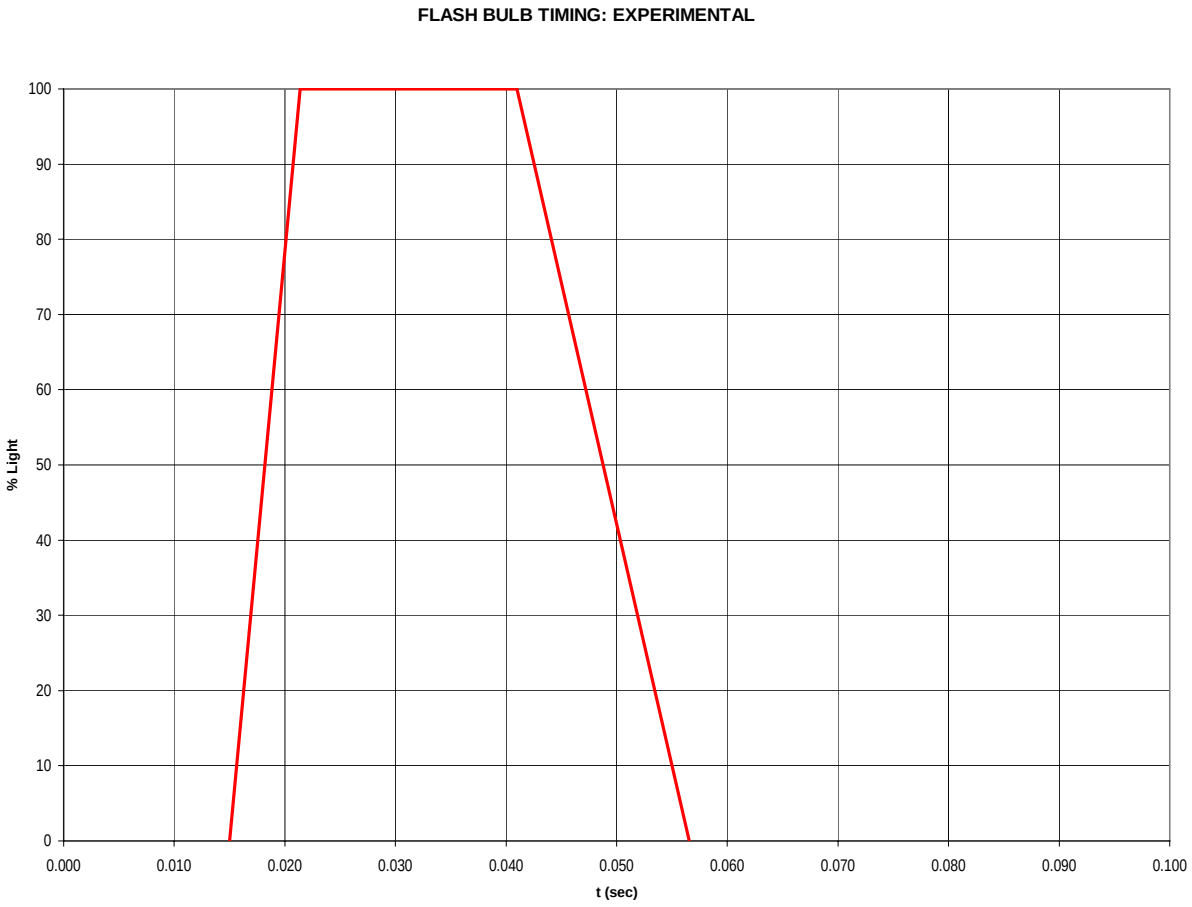


Figure C3: Flash Bulb Performance (Initiation at t=0)

APPENDIX B—COMPLETE TEST DATA

B.1 GENERALIZED COMPOSITE PANEL IMPACT DATA.

TABLE B-1. GENERALIZED COMPOSITE PANEL IMPACT RESULTS

Shot Number	Fragment Mass m (gm)	Fragment Length avg (x axis) (in)	Fragment Width avg (z axis) (in)	Fragment Maximum Thickness t_f (in)	Impact Velocity V_i (ft/s)	Residual Velocity V_r (ft/s)	Fragment yaw (deg)	Fragment pitch (deg)	Fragment roll (deg)	Fragment Impact Angle (deg)	Perimeter of Presented Area L (in)	Presented Area A_p (in^2)	Plate Thickness t (in)
25	244	7.688	2.938	0.250	512	441	26.9	-2.6	-17.0	63.6	12.8	10.0	0.060
26	244	7.688	2.938	1.250	383	311	34.8	-20.8	-13.4	51.5	15.7	14.1	0.060
27	244	7.688	2.938	2.250	214	166	3.6	-14.2	-55.1	76.3	9.8	5.4	0.060
30	244	7.688	2.938	3.250	223	143	180.0	-59.9	111.0	36.1	18.9	18.2	0.060
33	244	7.688	2.938	4.250	364	308	146.9	-169.5	119.6	82.2	13.7	3.1	0.060
34	244	7.688	2.938	5.250	342	299	0.0	5.6	0.0	90.0	10.2	5.7	0.060
35	244	7.688	2.938	6.250	154	88	90.7	-60.2	51.0	50.3	19.1	14.4	0.060
36	244	7.688	2.938	7.250	165	99	41.0	-12.5	-10.5	47.6	16.3	15.2	0.060
38	244	7.688	2.938	8.250	254	155	87.8	-48.6	25.3	26.9	20.6	20.1	0.060
39	244	7.688	2.938	9.250	473	409	-12.7	12.5	-16.1	74.3	10.5	6.1	0.060
40	244	7.688	2.938	10.250	470	409	26.2	-3.5	-11.5	63.7	12.7	10.0	0.060
41	244	7.688	2.938	11.250	308	270	16.7	0.4	-35.1	76.7	10.2	5.2	0.060
42	244	7.688	2.938	12.250	304	242	15.0	-22.9	-53.9	62.8	12.9	10.3	0.060
43	650	7.750	7.375	13.250	381	303	-32.5	18.8	14.9	63.3	22.9	25.7	0.060
44	650	7.750	7.375	14.250	307	225	63.9	-4.4	-3.6	26.0	28.7	51.4	0.060
47	650	7.750	7.375	15.250	406	358	15.5	1.5	14.9	74.7	18.9	15.1	0.060
48	650	7.750	7.375	16.250	248	193	88.4	16.9	-13.0	13.5	29.8	55.6	0.060
49	650	7.750	7.375	17.250	240	196	45.3	23.7	8.0	42.0	26.4	42.5	0.060
50	650	7.750	7.375	18.250	383	296	48.7	-13.4	-8.4	40.1	26.6	43.7	0.060
51	650	7.750	7.375	19.250	327	237	-52.0	16.9	-11.4	36.1	27.3	46.2	0.060
52	650	7.750	7.375	20.250	260	217	12.4	12.7	-51.2	88.1	18.9	3.5	0.060
53	650	7.750	7.375	21.250	351	255	63.6	-32.4	-15.0	22.1	29.1	53.0	0.060
54	650	7.750	7.375	22.250	311	229	60.5	2.9	26.5	37.8	27.2	45.1	0.060
55	650	7.750	7.375	23.250	237	111	82.2	14.0	2.5	7.6	30.1	56.7	0.060
56	244	7.688	2.938	24.250	270	185	-48.7	27.8	-25.7	35.9	18.4	18.3	0.060
57	244	7.688	2.938	25.250	269	227	22.0	-4.7	-43.2	71.0	11.7	7.4	0.060

TABLE B-2. GENERALIZED COMPOSITE PANEL IMPACT RESULTS

Shot Number	L (m)	A_p (m^2)	Dynamic Shear Modulus Gd (Pa)	Plate density rho (kg/m3)	t (m)	m (kg)	V_i (m/s)	V50 (m/s)	Penetration	Predicted V_r~ (m/s)	V_{50} (ft/s)	Predicted V_r~ (ft/s)	Q $1-(V_r-V_r\sim)/V_i$
25	0.326	0.00647	2.510E+08	1544.0	0.00152	0.24400	156.1	39.5	Yes	142.2	129.5	466.4	1.05
26	0.398	0.00907	2.510E+08	1544.0	0.00152	0.24400	116.7	43.6	Yes	99.5	143.1	326.6	1.04
27	0.248	0.00345	2.510E+08	1544.0	0.00152	0.24400	65.3	34.4	Yes	53.7	112.9	176.3	1.05
30	0.480	0.01177	2.510E+08	1544.0	0.00152	0.24400	68.1	47.9	Yes	43.4	157.1	142.5	1.00
33	0.347	0.00199	2.510E+08	1544.0	0.00152	0.24400	110.9	40.7	Yes	101.2	133.6	332.1	1.07
34	0.260	0.00370	2.510E+08	1544.0	0.00152	0.24400	104.2	35.2	Yes	94.7	115.6	310.6	1.03
35	0.486	0.00930	2.510E+08	1544.0	0.00152	0.24400	47.0	48.2	Yes	≈0*	158.2	≈0*	-
36	0.413	0.00984	2.510E+08	1544.0	0.00152	0.24400	50.2	44.4	Yes	21.4	145.8	70.3	0.82
38	0.524	0.01299	2.510E+08	1544.0	0.00152	0.24400	77.6	50.0	Yes	52.7	164.1	172.8	1.07
39	0.268	0.00394	2.510E+08	1544.0	0.00152	0.24400	144.1	35.8	Yes	134.5	117.3	441.4	1.07
40	0.323	0.00645	2.510E+08	1544.0	0.00152	0.24400	143.3	39.3	Yes	129.7	128.8	425.6	1.04
41	0.260	0.00336	2.510E+08	1544.0	0.00152	0.24400	93.7	35.3	Yes	84.1	115.7	276.0	1.02
42	0.328	0.00665	2.510E+08	1544.0	0.00152	0.24400	92.6	39.6	Yes	78.6	129.8	258.0	1.05
43	0.581	0.01659	2.510E+08	1544.0	0.00152	0.65000	116.1	32.3	Yes	105.2	105.9	345.3	1.11
44	0.729	0.03314	2.510E+08	1544.0	0.00152	0.65000	93.6	36.1	Yes	77.1	118.6	253.0	1.09
47	0.480	0.00975	2.510E+08	1544.0	0.00152	0.65000	123.9	29.3	Yes	116.2	96.3	381.4	1.06
48	0.758	0.03586	2.510E+08	1544.0	0.00152	0.65000	75.5	36.9	Yes	58.3	121.0	191.4	0.99
49	0.670	0.02740	2.510E+08	1544.0	0.00152	0.65000	73.1	34.7	Yes	58.5	113.7	192.0	0.98
50	0.676	0.02822	2.510E+08	1544.0	0.00152	0.65000	116.8	34.8	Yes	101.2	114.3	332.0	1.09
51	0.693	0.02980	2.510E+08	1544.0	0.00152	0.65000	99.7	35.3	Yes	84.2	115.7	276.3	1.12
52	0.479	0.00227	2.510E+08	1544.0	0.00152	0.65000	79.2	29.3	Yes	73.0	96.2	239.5	1.09
53	0.740	0.03418	2.510E+08	1544.0	0.00152	0.65000	106.9	36.4	Yes	89.4	119.5	293.3	1.11
54	0.692	0.02913	2.510E+08	1544.0	0.00152	0.65000	94.9	35.2	Yes	79.8	115.6	261.7	1.11
55	0.765	0.03655	2.510E+08	1544.0	0.00152	0.65000	72.3	37.0	Yes	54.8	121.5	179.8	1.29
56	0.466	0.01181	2.510E+08	1544.0	0.00152	0.24400	82.3	47.2	Yes	60.5	154.9	198.6	1.05
57	0.296	0.00474	2.510E+08	1544.0	0.00152	0.24400	82.0	37.6	Yes	69.7	123.5	228.7	1.01

B.2 2024-351 ALUMINUM PANEL IMPACT DATA.

TABLE B-3. 2024-T351 ALUMINUM PANEL IMPACT RESULTS

Shot Number	Fragment Mass m (gm)	Fragment Length avg (x axis) (in)	Fragment Width avg (z axis) (in)	Fragment Maximum Thickness t_f (in)	Impact Velocity V_i (ft/s)	Residual Velocity V_r (ft/s)	Fragment yaw (deg)	Fragment pitch (deg)	Fragment roll (deg)	Fragment Impact Angle (deg)	Perimeter of Presented Area L (in)	Presented Area A_p (in^2)	Plate Thickness t (in)
3	772	7.625	7.563	0.250	553	0	89.0	13.4	0.7	88.9	30.4	57.7	0.250
4	772	7.625	7.563	0.250	541	0	79.7	-12.0	-11.1	76.6	30.0	56.1	0.250
5	772	7.625	7.563	0.250	368	0	46.6	-8.8	-9.5	47.2	26.3	42.3	0.250
7	770	7.625	7.563	0.250	402	0	68.9	-2.9	1.8	68.7	29.3	53.7	0.250
8	770	7.625	7.563	0.250	499	0	-0.6	0.1	-27.1	0.6	16.1	3.8	0.375
9	748	7.125	7.938	0.250	588	0	89.0	20.0	0.0	89.0	30.1	56.6	0.375
10	748	7.125	7.938	0.250	608	0	33.0	55.6	51.3	61.7	28.4	49.8	0.375
23	715	7.625	7.750	0.250	603	229	3.5	4.4	39.6	5.5	17.0	5.7	0.375
24	748	7.125	7.938	0.250	554	0	23.6	6.3	34.2	22.8	21.6	22.0	0.375
64	741	7.750	7.375	0.250	445	0	-52.9	11.6	11.5	49.2	26.7	43.3	0.250
65	741	7.750	7.375	0.250	469	0	-41.6	-1.4	-10.4	40.6	24.9	37.2	0.250
66	650	7.750	7.375	0.250	563	207	32.9	-8.6	-5.6	33.6	23.4	31.6	0.250
67	679.1	7.750	7.375	0.250	536	339	-1.3	6.9	22.2	1.4	16.8	3.7	0.250
68	679.1	7.750	7.375	0.250	511	283	-14.2	-5.6	-14.0	12.4	18.7	12.3	0.250

TABLE B-4. 2024-T351 ALUMINUM PANEL IMPACT RESULTS*

Shot Number	L (m)	A_p (m^2)	Dynamic Shear Modulus Gd (Pa)	Plate density rho (kg/m3)	t (m)	m (kg)	V_i (m/s)	V50 (m/s)	Penetration	Predicted V_r~ (m/s)	V_{50} (ft/s)	Predicted V_r~ (ft/s)	Q $1-(V_r-V_r\sim)/V_i$
3	0.77	0.03720	2.760E+08	2771.5	0.006350	0.7720	168.6	149	No	42.57	489	140	1.25
4	0.76	0.03619	2.760E+08	2771.5	0.006350	0.7720	165.0	148	No	39.88	486	131	1.24
5	0.67	0.02731	2.760E+08	2771.5	0.006350	0.7720	112.3	139	No	≈0*	456	≈0*	-
7	0.75	0.03466	2.760E+08	2771.5	0.006350	0.7700	122.4	147	No	≈0*	482	≈0*	-
8	0.41	0.00244	2.760E+08	2771.5	0.009525	0.7700	152.2	163	No	≈0*	536	≈0*	-
9	1.44	0.01944	2.760E+08	2771.5	0.009525	0.7480	179.3	310	No	≈0*	1017	≈0*	-
10	0.72	0.03213	2.760E+08	2771.5	0.009525	0.7480	185.2	220	No	≈0*	721	≈0*	-
23	0.43	0.00367	2.760E+08	2771.5	0.009525	0.7150	183.9	174	Yes	52.40	571	172	0.91
24	0.55	0.01416	2.760E+08	2771.5	0.009525	0.7480	168.9	192	No	≈0*	629	≈0*	-
64	0.68	0.02794	2.760E+08	2771.5	0.006350	0.7410	135.7	143	No	≈0*	468	≈0*	-
65	0.63	0.02399	2.760E+08	2771.5	0.006350	0.7410	142.9	138	No	24.00	452	79	1.17
66	0.59	0.02040	2.760E+08	2771.5	0.006350	0.6500	171.6	143	Yes	61.59	468	202	0.99
67	0.43	0.00236	2.760E+08	2771.5	0.006350	0.6791	163.4	118	Yes	106.26	388	349	1.02
68	0.47	0.00793	2.760E+08	2771.5	0.006350	0.6791	155.8	125	Yes	77.43	409	254	0.94

*Cases where $V_{50} > V_i$ produce imaginary results from the penetration equation; the implication is that no penetration is predicted.

B.3 Ti-6Al-4V TITANIUM PANEL IMPACT DATA.

TABLE B-5. Ti-6Al-4V TITANIUM PANEL IMPACT RESULTS

Shot Number	Fragment Mass m (gm)	Fragment Length avg (x axis) (in)	Fragment Width avg (z axis) (in)	Fragment Maximum Thickness t_f (in)	Impact Velocity V_i (ft/s)	Residual Velocity V_r (ft/s)	Fragment yaw (deg)	Fragment pitch (deg)	Fragment roll (deg)	Fragment Impact Angle (deg)	Presented Area A_p (in^2)	Perimeter of Presented Area L (in)	Plate Thickness t (in)
Pre0	800.0	7.500	7.313	0.250	0	0	-	-	-	-	0.0	0.0	0.063
Pre1	800.0	7.500	7.313	0.250	0	0	-	-	-	-	0.0	0.0	0.063
Pre2	800.0	7.500	7.313	0.250	647	442	-77.8	-2.7	28.6	30.3	27.7	47.3	0.063
Pre3	767.0	7.625	7.563	0.250	427	294	100.6	-22.0	40.4	37.5	27.3	45.7	0.063
Pre4	740.0	7.125	7.813	0.250	309	246	-0.1	-12.6	23.7	84.8	18.6	5.0	0.063
11.0	740.0	7.125	7.813	0.250	426	155	0.7	11.3	22.6	85.0	18.3	4.8	0.125
12.0	740.0	7.125	7.813	0.250	406	212	-3.4	-0.1	26.7	86.9	16.7	3.9	0.125
13.0	738.0	7.250	7.813	0.250	379	8	24.2	-11.6	6.5	67.2	21.0	21.7	0.125
14.0	714.0	7.250	7.813	0.250	341	0	4.3	2.4	-153.0	85.1	16.9	4.9	0.125
15.0	714.0	7.250	7.813	0.250	365	0	4.1	2.5	28.5	85.2	16.8	4.7	0.125
16.0	714.0	7.250	7.813	0.250	723	211	-2.6	6.9	-162.5	89.5	17.6	3.9	0.250
17.0	703.0	7.625	7.563	0.250	780	269	0.7	1.5	-37.1	89.7	16.2	3.8	0.250
18.0	723.0	7.125	7.875	0.250	501	0	42.5	0.0	0.0	47.5	41.4	26.1	0.250
19.0	680.0	6.375	7.500	0.250	495	0	-56.6	25.0	-19.5	30.1	26.0	41.4	0.250
20.0	702.0	7.125	7.250	0.250	748	8	-1.7	1.7	15.5	88.8	15.6	3.6	0.250
21.0	639.0	6.000	7.500	0.250	781	0	-0.5	6.5	38.3	86.4	33.1	3.7	0.250
22.0	577.0	6.500	7.125	0.250	871	0	-0.2	-0.1	21.4	89.8	30.5	3.6	0.250

TABLE B-6. Ti-6Al-4V TITANIUM PANEL IMPACT RESULTS

Shot Number	L (m)	A_p (m^2)	Dynamic Shear Modulus Gd (Pa)	Plate density rho (kg/m3)	t (m)	m (kg)	V_i (m/s)	V50 (m/s)	Penetration	Predicted V_r~ (m/s)	V_{50} (ft/s)	Predicted V_r~ (ft/s)	Q $1-(V_r-V_r\sim)/V_i$
Pre0	0.000	0.00000	9.000E+08	4770.0	0.00160	0.8000	0.00	0.00	No	≈0*	0	≈0*	-
Pre1	0.000	0.00000	9.000E+08	4770.0	0.00160	0.8000	0.00	0.00	No	≈0*	0	≈0*	-
Pre2	0.703	0.03054	9.000E+08	4770.0	0.00160	0.8000	197.22	63.63	Yes	144.55	209	474	1.1
Pre3	0.694	0.02951	9.000E+08	4770.0	0.00160	0.7670	130.04	64.56	Yes	87.25	212	286	1.0
Pre4	0.471	0.00324	9.000E+08	4770.0	0.00160	0.7400	94.06	54.18	Yes	74.39	178	244	1.0
11.0	0.465	0.00310	9.000E+08	4770.0	0.00318	0.7400	129.98	106.80	Yes	69.66	350	229	1.2
12.0	0.425	0.00252	9.000E+08	4770.0	0.00318	0.7400	123.73	102.10	Yes	66.47	335	218	1.0
13.0	0.535	0.01402	9.000E+08	4770.0	0.00318	0.7380	115.38	114.65	Yes	10.09	376	33	1.1
14.0	0.124	0.01089	9.000E+08	4770.0	0.00318	0.7140	103.89	56.04	No	71.06	184	233	1.7
15.0	0.428	0.00303	9.000E+08	4770.0	0.00318	0.7140	111.27	104.23	No	36.59	342	120	1.3
16.0	0.098	0.01136	9.000E+08	4770.0	0.00635	0.7140	220.41	100.01	Yes	132.55	328	435	1.3
17.0	0.412	0.00244	9.000E+08	4770.0	0.00635	0.7030	237.68	206.19	Yes	106.99	677	351	1.1
18.0	1.052	0.01681	9.000E+08	4770.0	0.00635	0.7230	152.58	324.91	No	≈0*	1066	≈0*	-
19.0	0.661	0.02668	9.000E+08	4770.0	0.00635	0.6800	150.87	265.63	No	≈0*	872	≈0*	-
20.0	0.397	0.00234	9.000E+08	4770.0	0.00635	0.7020	227.85	202.57	Yes	94.75	665	311	1.4
21.0	0.841	0.00240	9.000E+08	4770.0	0.00635	0.6390	238.10	309.14	No	≈0*	1014	≈0*	-
22.0	0.775	0.00230	9.000E+08	4770.0	0.00635	0.5770	265.56	312.17	No	≈0*	1024	≈0*	-

*Cases where $V_{50} > V_i$ produce imaginary results from the penetration equation; the implication is that no penetration is predicted.

B.4 INCONEL® 625 LCF PANEL IMPACT DATA.

TABLE B-7. INCONEL® 625 LCF PANEL IMPACT RESULTS

Shot Number	Fragment Mass m (gm)	Fragment Length avg (x axis) (in)	Fragment Width avg (z axis) (in)	Fragment Maximum Thickness t_f (in)	Impact Velocity V_i (ft/s)	Residual Velocity V_r (ft/s)	Fragment yaw (deg)	Fragment pitch (deg)	Fragment roll (deg)	Fragment Impact Angle (deg)	Perimeter of Presented Area L (in)	Presented Area A_p (in^2)	Plate Thickness t (in)
58	650	7.750	7.375	0.250	418	308	23.8	-8.8	-5.3	24.5	21.29	23.67	0.063
59	650	7.750	7.375	0.250	434	0	47.4	-10.0	-12.4	48.1	26.30	42.55	0.063
60	650	7.750	7.375	0.250	458	298	-20.6	-16.5	8.7	22.8	21.28	22.20	0.063
61	650	7.750	7.375	0.250	424	294	-1.1	3.2	42.8	1.4	16.06	3.68	0.063
62	650	7.750	7.375	0.250	366	253	-3.7	14.1	15.5	0.2	18.31	3.57	0.063
63	741	7.750	7.375	0.250	340	0	41.1	4.1	-11.0	39.4	24.73	36.27	0.063

TABLE B-8. INCONEL® 625 LCF PANEL IMPACT RESULTS*

Shot Number	L (m)	A_p (m^2)	Dynamic Shear Modulus Gd (Pa)	Plate density rho (kg/m3)	t (m)	M (kg)	V_i (m/s)	V50 (m/s)	Penetration	Predicted V_r~ (m/s)	V_{50} (ft/s)	Predicted V_r~ (ft/s)	Q $1-(V_r-V_r\sim)/V_i$
58	0.541	0.01527	1.200E+09	8442	0.00160	0.650	127.47	71.50	Yes	80.11	234.59	262.83	0.89
59	0.668	0.02745	1.200E+09	8442	0.00160	0.650	132.29	79.47	No	67.34	260.73	220.95	1.51
60	0.540	0.01432	1.200E+09	8442	0.00160	0.650	139.56	71.48	Yes	92.37	234.54	303.06	1.01
61	0.408	0.00237	1.200E+09	8442	0.00160	0.650	129.37	62.11	Yes	108.15	203.77	354.83	1.14
62	0.465	0.00230	1.200E+09	8442	0.00160	0.650	111.68	66.31	Yes	85.76	217.56	281.39	1.08
63	0.628	0.02340	1.200E+09	8442	0.00160	0.741	103.54	72.18	No	52.04	236.83	170.74	1.50

*Cases where $V_{50} > V_i$ produce imaginary results from the penetration equation; the implication is that no penetration is predicted.